Am J Transl Res 2023;15(6):4291-4313
www.ajtr.org /ISSN:1943-8141/AJTR0148992

Original Article

Whole-transcriptome sequencing with ceRNA regulation network construction and verification in glioblastoma

Zhao-Mu Zeng[1,2,3*], Yue-Yue Chen[4*], Xi-Chao Wen[2*], Xiu-Chao Geng[5], Yi-Xi Zhu[6], Liang-Chao Hao[7], Zi-Shu Dong[8], Ji-Feng Yang[3], Ting-Ting Wang[3], Ruo-Bing Zhang[3], Zhi-Wei Sun[3,4], Yu-Hao Zhang[9], Ke-Bin Zheng[2]

[1]Department of Neurosurgery, Jiangxi Provincial People's Hospital, The First Affiliated Hospital of Nanchang Medical College, Nanchang 330000, Jiangxi, PR China; [2]Department of Neurosurgery, Affiliated Hospital of Hebei University, Baoding 071000, Hebei, PR China; [3]Department of Surgery, School of Clinical Medicine, Hebei University, Baoding 071000, Hebei, PR China; [4]Department of Toxicology and Sanitary Chemistry, School of Public Health, Capital Medical University, Beijing 100069, PR China; [5]Department of Nursing, School of Medicine, Taizhou University, Jiaojiang 318000, Zhejiang, PR China; [6]Department of Pharmacy, The Second Affiliated Hospital of Nanchang University, Nanchang 330000, Jiangxi, PR China; [7]Department of Plastic Surgery, Shaoxing People's Hospital, Shaoxing 312000, Zhejiang, PR China; [8]Department of Zoology, Advanced Research Institute, Jiangxi University of Chinese Medicine, Nanchang 330000, Jiangxi, PR China; [9]Cancer Center, Department of Neurosurgery, Zhejiang Provincial People's Hospital, Affiliated to Hangzhou Medical College, Hangzhou 310000, Zhejiang, PR China. [*]Equal contributors.

Received January 6, 2023; Accepted May 22, 2023; Epub June 15, 2023; Published June 30, 2023

Abstract: Objectives: To explore the key genes involved in the occurrence and development of glioblastoma (GBM) by analyzing whole-transcriptome sequencing and biologic data from GBM and normal cerebral cortex tissues and to search for important noncoding RNA (ncRNA) molecular markers based on the competitive endogenous RNA (ceRNA) network. Methods: Ten GBM and normal cerebral cortex tissues were collected for full transcriptome sequencing, screened for differentially expressed (DE) mRNAs, miRNAs, lncRNAs, and circRNAs, and subjected to bioinformatic analysis. We constructed a Protein-Protein Interaction (PPI) network and a circRNA/lncRNA-miRNA-mRNA regulatory network and identified them using reverse transcription-quantitative polymerase chain reaction (RT-qPCR). Finally, The Cancer Genome Atlas (TCGA) and Chinese Glioma Genome Atlas (CGGA) databases were used to validate and conduct a survival analysis of the target genes. Results: A total of 5341 DEmRNAs, 259 DEmiRNAs, 3122 DElncRNAs, and 2135 DEcircRNAs were identified. Enrichment analysis showed that target genes regulated by DEmiRNA, DElncRNA, and DEcircRNA were closely related to chemical synaptic transmission and ion transmembrane transport. A PPI network analysis screened 10 hub genes that directly participate in tumor cell mitosis regulation. In addition, the ceRNA composite network showed that hsa-miR-296-5p and hsa-miR-874-5p were the central nodes of the network, and the reliability of relevant key molecules was successfully verified through RT-qPCR identification and the TCGA database. The CGGA database survival analysis produced 8 DEmRNAs closely related to GBM patient survival prognosis. Conclusions: This study revealed the important regulatory functions and molecular mechanisms of ncRNA molecules and identified hsa-miR-296-5p and hsa-miR-874-5p as key molecules in the ceRNA network. They may play an important role in GBM pathogenesis, treatment, and prognosis.

Keywords: Glioblastoma, whole-transcriptome sequencing, ceRNA network, hub genes, hsa-miR-296-5p, hsa-miR-874-5p

Introduction

Gliomblastma (GBM) is known as a "brain killer" and is one of the most aggressive malignant solid tumors. It accounts for 48% of primary malignant tumors of the central nervous system. Relapse after treatment is common in GBM, making it highly fatal [1, 2]. Although a series of significant advances have been made in molecular-targeted therapy, immunotherapy, and other treatment strategies for GBM, the prognosis of GBM patients is still poor, and the median survival time after diagnosis is only 1-1.5 years [1, 3, 4]. The main reason is that there is a poor understanding of the complex GBM regulatory process, which involves multiple factors and elements, and there are no reliable tools for early diagnosis and treatment

monitoring. Therefore, the molecular mechanisms underlying the occurrence and development of GBM are key scientific problems that urgently need to be solved in the clinical treatment of GBM. In short, if we use efficient bioinformatic analytical methods to reveal the pathogenic mechanism of GBM and screen out the core genes related to GBM, this will open up more possibilities for precise treatment and will bring more benefit to the clinical diagnosis and treatment.

The publication of the draft of the human genome in 2001 marked the moment when human beings obtained their own "book of nature". In the human genome, less than 2% of DNA can encode proteins. Much of the other 98% of the DNA is only transcribed into RNA and cannot be further translated into protein [5, 6]. Our understanding of ncRNA is still in its early stages. ncRNAs not only act as regulatory factors and play key roles in tumor proliferation, invasion, apoptosis, autophagy, and immune response but also are specific biomarkers that have broad clinical application prospects in assisted diagnosis of tumors, treatment guidance, and prognostic assessment [7-10]. In recent years, high-throughput sequencing technology and bioinformatic analysis have completely changed the research methods of biomedicine and other disciplines. Through RNA sequencing (RNA-Seq), thousands of ncRNAs, mainly microRNAs (miRNAs), long noncoding RNAs (lncRNAs), and circular RNAs (circRNAs), have been identified [11, 12]. The ceRNA hypothesis reveals a new mechanism of RNA interaction, which represents a new gene expression regulatory mode. Compared to miRNA networks, ceRNA regulatory networks are more elaborate and complex and involve many types of RNA molecules (mRNAs, pseudogene transcripts, lncRNAs, and circRNAs) [13, 14]. Such RNA molecules with common miRNA response elements can affect the biologic characteristics of tumors by competitively binding to miRNAs [15]. Therefore, ceRNA regulatory network analysis provides a new perspective from which researchers can carry out whole-transcriptome studies, which will help to comprehensively explain the biologic phenomena of tumors.

In this study, we used whole-transcriptome sequencing technology to screen five groups of tumor tissues (diagnosed as GBM after postoperative pathology) and normal cerebral cortical tissues (cerebral herniation caused by traumatic brain contusion, requiring internal decompression) to find differentially expressed mRNAs, miRNAs, lncRNAs, and circRNAs. Data were visualized and analyzed by bioinformatic methods and functional interaction prediction for DEmRNA data under different conditions. Finally, a ceRNA regulatory network composed of circRNAs, lncRNAs, miRNAs, and mRNAs was constructed using the key molecules miR-296-5p and miR-874-5p in the network as the entry points to select ceRNAs that had complementary pairing relationships with them. RT-qPCR and survival analysis were performed to verify the roles of these ceRNAs. Therefore, our results not only provide new evidence for the ceRNA regulatory network related to the pathogenesis of GBM but also provide possible biomarkers for precise treatment and prognosis of GBM.

Materials and methods

Patients and sample collection

GBM tissues (confirmed to be GBM by postoperative pathological diagnosis) and normal cerebral cortex tissues (from patients with traumatic brain contusions and lacerations combined with cerebral hernias requiring internal decompression) were collected intraoperatively. After the samples were isolated, they were rinsed with normal saline and immediately transferred to a 1.8-ml RNA-free cryopreserved tube, which was stored at -80°C. Five clinical samples from the GBM group (C) and normal control group (N) were selected for whole-transcriptome sequencing, and the remaining samples were stored for verification (Table S1). Ethical approval for this study was obtained from the Ethics Committee of the Affiliated Hospital of Hebei University, and written informed consent was received from all participants (No. HDFY-LL-2022-046).

Whole-transcriptome library construction and sequencing

First, RNA was isolated with TRIzol reagent (Invitrogen, Grand Island, NY), and total RNA was purified by the Qiagen RNeasy mini kit (Qiagen, Valencia, CA). Purified RNA was ana-

lyzed on an ND-8000 spectrophotometer (NanoDrop Technologies, Wilmington, DE). High-quality total RNA was used as the starting material. Briefly, total RNA was used to remove ribosomal RNAs (rRNAs) with the NEBNext rRNA Depletion Kit (New England Biolabs, Inc., Massachusetts, USA) following the manufacturer's instructions. RNA libraries were constructed using the NEBNext® Ultra™ II Directional RNA Library Prep Kit (New England Biolabs, Inc., Massachusetts, USA) according to the manufacturer's instructions. Libraries were controlled for quality and quantified using the BioAnalyzer 2100 system (Agilent Technologies, Inc., USA). Library sequencing was performed on an Illumina NovaSeq 6000 instrument with 151-bp paired end reads.

microRNA library construction and sequencing

Total RNA was isolated with TRIzol reagent (Invitrogen, Grand Island, NY). Total RNA was analyzed on an ND-8000 spectrophotometer (NanoDrop, Technologies, Wilmington, DE) by agarose electrophoresis or using a 2100 Bioanalyzer (Agilent Technologies, Santa Clara, CA) for quantification. RNA samples were used if no smear was present on the agarose gel. RNA samples were also used if the 260/280 ratio was above 2.0 and the RNA integrity number (RIN) was greater than 7.0. High-quality total RNA (1 μg) was used as the starting material. The TruSeq small RNA sample preparation kit was used for 3' adaptor ligation, 5' adaptor ligation, reverse transcription, PCR amplification, and PAGE-purified small RNA library construction. Quality control and sequencing steps were the same as those described in section 2.2.

Whole-transcriptome sequencing data analysis

Briefly, fastp [16] software (v0.20.0) was used to trim adaptors and remove low-quality reads to obtain high-quality clean reads. STAR [17] software (v2.7.9a) was used to align the high-quality clean reads to the human reference genome (hg38). FeatureCounts [18] (v2.0), HTSeq [19] (v0.13.5), and DCC [20] (v0.5.0) software were used to obtain raw gene-level RNA read counts and determine the RNA expression profile (mRNA, lncRNA, and circRNA). As a high-throughput sequencing difference analysis method, DESep2 [21] can interpret potential confounding factors through generalized linear models, and has a good estimate of gene expression variance based on the negative binomial distribution's dispersion parameter. DESeq2 [21] software (v1.30.1) was used to normalize and calculate fold changes and *P* values between two groups. DERNAs with a fold change ≥ 2 that met the significance threshold $P < 0.05$ were considered significant. The Ensembl GTF gene annotation database (v104) was used to annotate the RNAs. ClusterProfiler [22] is an enrichment analysis software that judges enrichment items based on Over-Representation Analysis. Gene Ontology (GO) and Kyoto Encyclopedia of Genes and Genomes (KEGG) pathway enrichment analyses were performed with the clusterProfiler R package (v3.18.1) based on the DERNAs. rMATS [23] software (v4.1.1) was used to predict alternative between-group splicing events. A heatmap was drawn for the DEmRNAs, DEmiRNAs, DElncRNAs, and DEcircRNAs using the pheatmap R package (https://cran.r-project.org/web/packages/pheatmap/).

microRNA sequencing data analysis

First, fastp software was used to trim adaptors and filter low-quality reads to obtain high-quality clean reads. Then, clean reads from all samples were merged, and miRDeep2 [24] software (v0.1.3) was used to predict novel miRNAs. The clean reads were then aligned to the merged human miRNA databases (miRNA from miRbase v22.1 plus the newly predicted novel miRNAs) using Novoalign software (v3.09.04) with at most one mismatch. The mapped miRNA read counts were defined as the raw expression levels of that miRNA. The read counts were then normalized by DESeq2 R packages.

PPI network and module analysis of DEmRNAs

The interaction between DEG-encoded proteins was analyzed by STRING [25] (version 11.5; https://cn.string-db.org/) using stringApp (version 1.7.0; https://apps.cytoscape.org/apps/stringapp) in Cytoscape [26]. The input gene set was set as all DEGs, and the species was set as human. To determine the most closely related interaction pairs, we set the PPI score to 0.99 (high confidence). Cytoscape's plug-in MCODE [27] (version 2.0.0; https://apps.cytoscape.org/apps/mcode) was used to analyse the most significant clustering modules in the

PPI network, and we set the node score cut-off to 0.3. The significant clustering module gene was also subjected to gene ontology-biological process (GO-BP) enrichment analysis. The GO-BP terms with enriched gene counts ≥ 2 that met the significance threshold $P < 0.05$ were considered significant.

Prediction of miRNA regulatory relationships

MiRNA-gene, miRNA-lncRNA, and miRNA-circRNA regulatory relationships were determined using miRanda [28] software and TargetScan [29] software. To identify the most closely related interaction pairs, we set the Context+ threshold in TargetScan to -0.48 and the structure score threshold in miRanda to 140. The predicted miRNA-lncRNA and miRNA-circRNA regulatory relationships were integrated with DElncRNAs and DEcircRNAs to determine the DEmiRNA-DElncRNA regulatory relationship and DEmiRNA-DEcircRNA regulatory relationship. Cytoscape was applied to build a ceRNA network.

RT-qPCR validation and TCGA GBM data validation

To validate the transcriptome data, the expression levels of selected genes (circRNAs, miRNAs, lncRNAs, and mRNAs) were analysed with RT-qPCR. The same samples used for RNA-Seq were reverse transcribed into cDNA using random primers for mRNAs and lncRNAs, divergent primers for circRNAs, and bulge-loop primers for miRNAs. All primers were synthesized by NewCore Biotech (Shanghai, China). The primer sequences are listed in Table S2. The GAPDH gene was used as the reference gene for circRNAs, lncRNAs, and mRNAs, and U6 snRNA was used as the reference gene for miRNAs. All reactions were run in triplicate and are presented as the mean ± standard error of the means (S.E.M). Student's t test was used to compare expression levels among different groups. Genomic Data Commons (GDC) TCGA GBM data provided by the University of California Santa Cruz (UCSC) Xena database (https://xenabrowser.net/datapages/) were used in this study for data validation.

Statistical analysis

The mean ± standard deviation (SD) was calculated from the data of three independent experiments. Statistical tests were conducted using SPSS 25.0 and GraphPad Prism 7.0 software. Paired Student's t tests were performed between the GBM group and the normal control group samples. One-way ANOVA was utilized to compare differences among three or more groups. All experiments were repeated three times independently. Data were considered significant as follows: $*P$-value < 0.05, $**P$-value < 0.01, and $***P$-value < 0.001.

Results

Differential expression analysis

In this study, whole-transcriptome sequencing data (circRNAs, lncRNAs, miRNAs, and mRNAs) from five groups of GBM tissue (C) and normal cortical tissue (N) samples were obtained by the Illumina NovaSeq 6000 sequencing platform, and a series of DEncRNAs and DEmRNAs were identified based on screening criteria. There were 5341 DEmRNAs (2255 upregulated, 3086 downregulated), 259 DEmiRNAs (116 upregulated, 143 downregulated), 3122 DElncRNAs (1130 upregulated, 1992 downregulated), and 2135 DEcircRNAs (628 upregulated, 1507 downregulated). In addition, the volcano plots and two-way clustering heatmaps of DEmRNAs, DEmiRNAs, DElncRNAs, and DEcircRNAs are shown in **Figure 1**. From this, we observed that the tumor samples were significantly separated from the paracancerous samples, and the expression profiles of various genes were also significantly different, which indicated that our sequencing data were reliable. According to the statistical calculations, the mRNA with the highest upregulation was HOXD10 (1075-fold change), and the mRNA that was most downregulated was NPAS4 (926-fold change). In addition, the most upregulated miRNAs, lncRNAs, and circRNAs were hsa-miR-10b-5p (824-fold change), lncRNA-ENST00000440016 (796-fold change), and hsa_circ_0000992 (93-fold change), respectively. The most downregulated miRNAs, lncRNAs, and circRNAs were hsa-miR-873-3p (213-fold change), lncRNA-ENST00000501520 (724-fold change), and chr12:1289852-1410453+ (novel circRNA, 118-fold change), respectively. Tables S3, S4, S5, S6 show the details of the top 10 differentially up- and down-regulated DEmRNAs, DEmiRNAs, DElncRNAs, and DEcircRNAs.

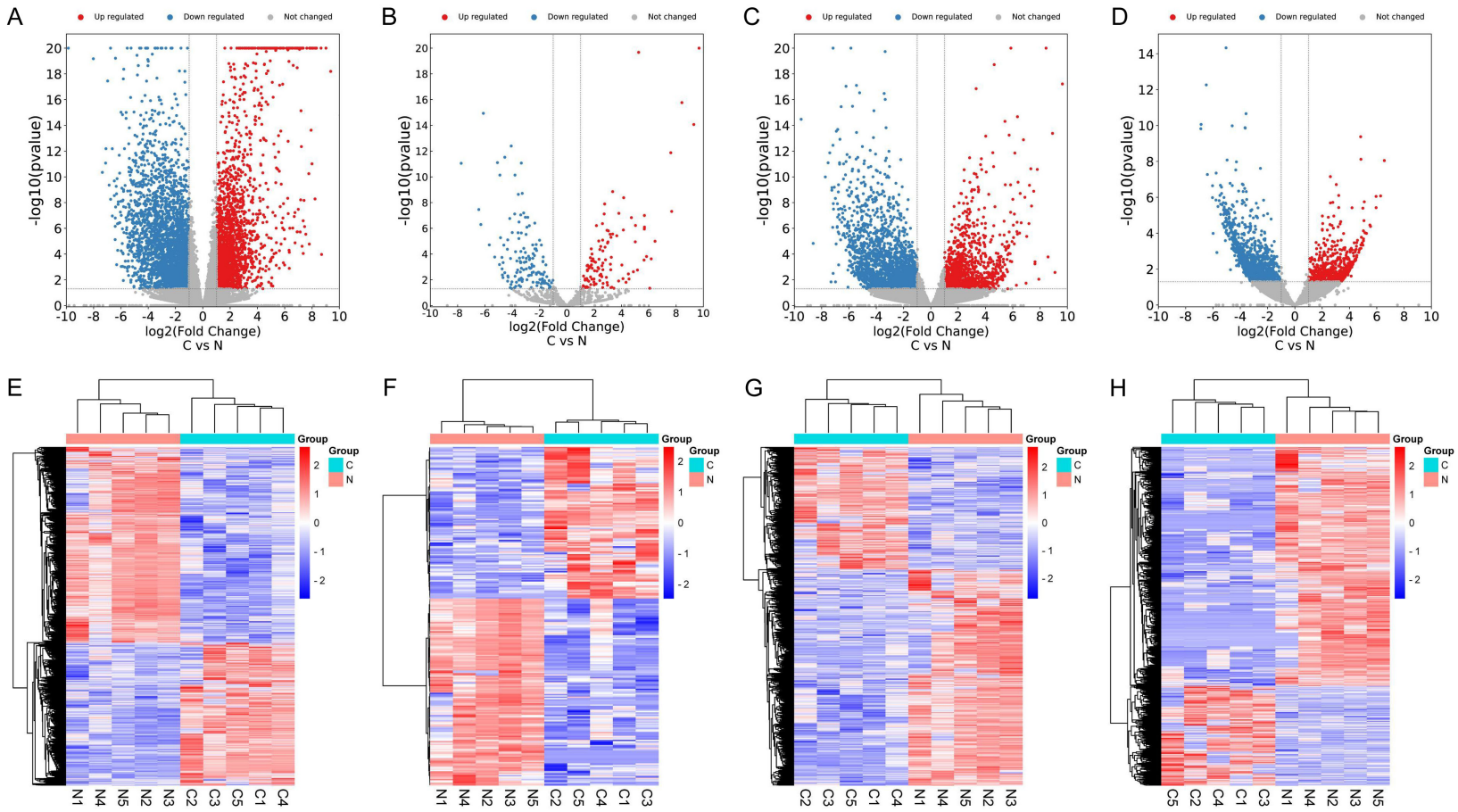

Figure 1. Volcano plot and clustering heat maps of differentially expressed molecules in tumour and paracancerous tissues. A. DEmRNA volcano plot; B. DEmiRNA volcano plot; C. DElncRNA volcano plot; D. DEcircRNA volcano plot. Red dots indicate upregulated genes, blue dots indicate downregulated genes, and grey dots indicate no differences. E. Heat map of DEmRNA clustering; F. Heat map of DEmiRNA clustering; G. Heat map of DElncRNA clustering; H. Heat map of DEcircRNA clustering. Red indicates upregulation, and blue indicates downregulation.

Functional enrichment analysis of DEmRNAs

To better understand the GBM biological process and the involved regulatory mechanisms, we performed GO-BP functional analysis and KEGG pathway enrichment analysis on the DEmRNAs. The results showed that 1597 GO-BP terms were enriched among the upregulated genes, and that 1098 GO-BP terms were enriched among the downregulated genes. In addition, upregulated genes were enriched in 42 KEGG pathways, and downregulated genes were enriched in 34 KEGG pathways. **Figure 2A-D** shows only the top 20 GO-BP terms and KEGG signaling pathways that were characterized by upregulation or downregulation of DEmRNAs. In addition, the GO-BP and KEGG data showed that the functions of upregulated genes were mainly related to nucleosome assembly (GO: 0006334), DNA conformation change (GO: 0071103), extracellular matrix organization (GO: 0030198), systemic lupus erythematosus (KEGG: hsa05322) and the cell cycle (KEGG: hsa04110). Downregulated genes were mainly related to the modulation of chemical synaptic transmission (GO: 0050804), regulation of membrane potential (GO: 0042391), regulation of ion transmembrane transport (GO: 0034765), neuroactive ligand-receptor interaction (KEGG: hsa04080), and calcium signaling (KEGG: hsa04020).

Enrichment analysis of DEmiRNA-, DElncRNA-, and DEcircRNA-related target genes

To better understand the biological changes and regulatory mechanisms involved in each interaction during the malignant progression of GBM, we selected the DEmRNAs based on the following three regulatory relationships: DEmiRNA-DEmRNA, DElncRNA-DEmRNA, and DEcircRNA-DEmRNAs. The results of the GO-BP and KEGG enrichment analyses of these DEmRNAs are shown in **Figure 3** in bar graphs and bubble charts. GO-BP enrichment analysis showed that the functions involving the modulation of chemical synaptic transmission (GO: 0050804), regulation of ion transmembrane transport (GO: 0034765) and regulation of membrane potential (GO: 0042391) were the main functions enriched in the target genes related to the DEmiRNAs, DElncRNAs, and DEcircRNAs (**Figure 3A-C**). In the KEGG pathway enrichment analysis (**Figure 3D-F**), we identified 122 enriched pathways based on the DEmiRNA-DEmRNA regulatory relationship, of which calcium signalling (hsa04020) and mitogen-activated protein kinase (MAPK) signalling (hsa04010) were the most enriched. There were 90 pathways of genes based on the coexpression of DElncRNA-DEmRNA, which were mainly closely related to the neuroactive ligand-receptor (hsa04080) and glutamatergic synapse (hsa04724). One hundred pathways-mainly neuroactive ligand-receptor interaction (hsa04080) and cyclic adenosine monophosphate (cAMP) signalling (hsa04024)-were enriched in genes identified through the DEcircRNA-DEmRNA coexpression relationship.

Recognition of core DEmRNAs in the PPI network

To further study the functions of genes at the protein level, we selected DEmRNAs based on the DEmiRNA-DEmRNA regulatory relationship and the coexpression relationship of DElncRNA-DEmRNA and DEcircRNA-DEmRNA to construct a PPI network consisting of 503 nodes and 1489 interaction pairs (confidence cut-off: 0.99), and the interactions between 503 DEmRNAs (364 upregulated and 139 downregulated) were examined by removing unconnected nodes. In this PPI network, the nodes with high topological scores were considered key nodes of the network. We used the Cytoscape Molecular Complex Detection (MCODE) plug-in to select four subnetwork modules, and the involved DEmRNAs were all upregulated genes, which are also marked in **Figure 4A** using differently colored rings. According to the statistical results, Module A (score = 31) contained 31 nodes and 465 interaction pairs, of which ribosomal proteins, such as ribosomal protein S8 (RPS8, degree = 34), RPS3A (degree = 32), and RPS27 (degree = 28), were the most abundant. Module B (score = 14) had 21 nodes and 140 interaction pairs, mainly including minichromosome maintenance protein 2 (MCM2, degree = 26), MCM7 (degree = 24) and MCM4 (degree = 24). Module C (score = 8.6) had 11 nodes and 43 interaction pairs, including many cell cycle-related proteins, such as cyclin-dependent kinase 1 (CDK1, degree = 45) and cell division cycle protein 20 (CDC20, degree = 25). Module D (score = 3.5) had 12 nodes and 19 interaction pairs. These genes were closely related to the regulation of mitosis and mainly included

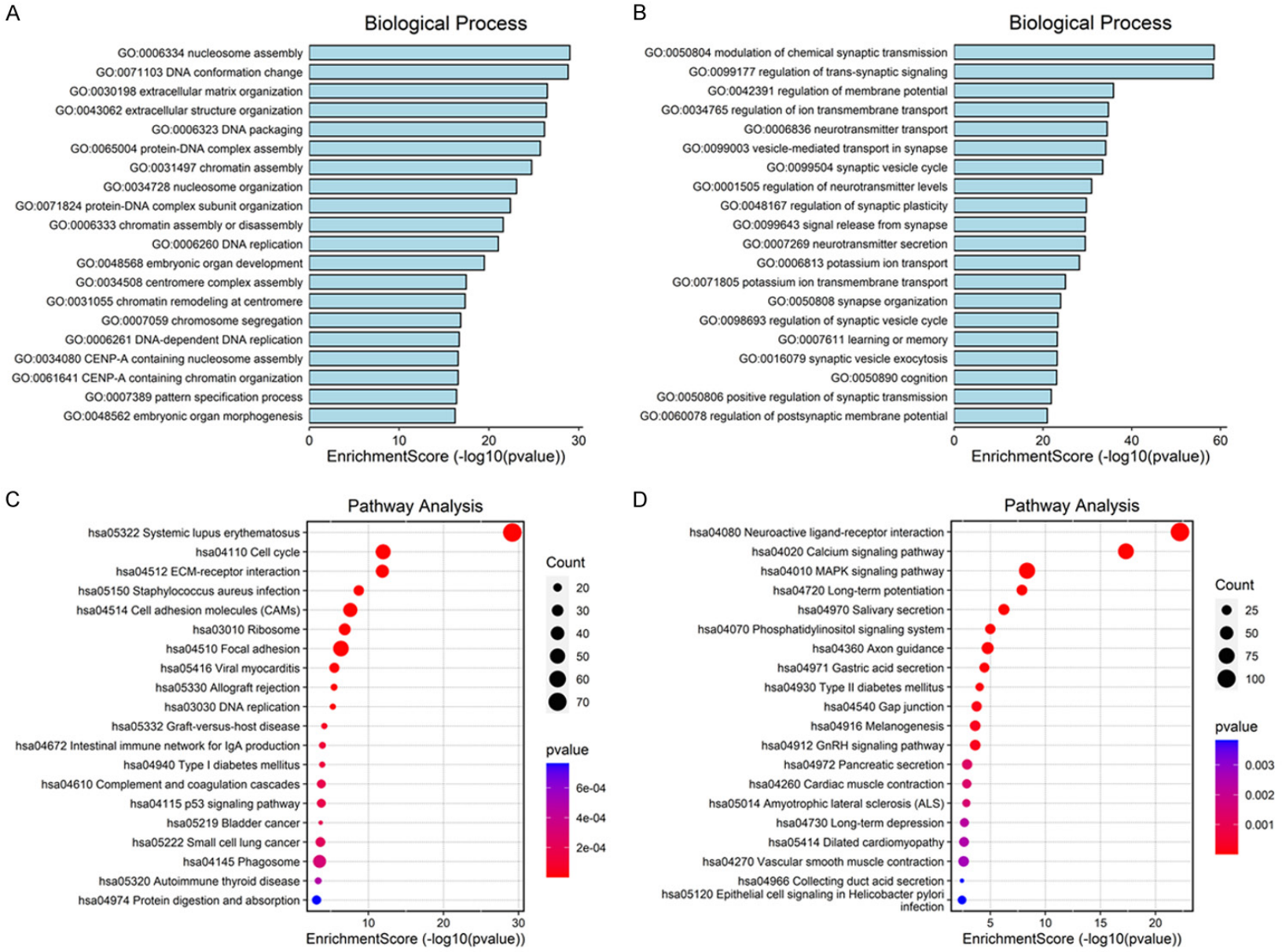

Figure 2. DEmRNA GO-BP and KEGG pathway enrichment analyses. A. Upregulation of the top 20 GO-BP terms for DEmRNA enrichment; B. Downregulation of the top 20 GO-BP terms for DEmRNA enrichment; C. Upregulation of the top 20 KEGG signaling pathways for DEmRNA enrichment; D. Downregulation of the top 20 KEGG signaling pathways for DEmRNA enrichment.

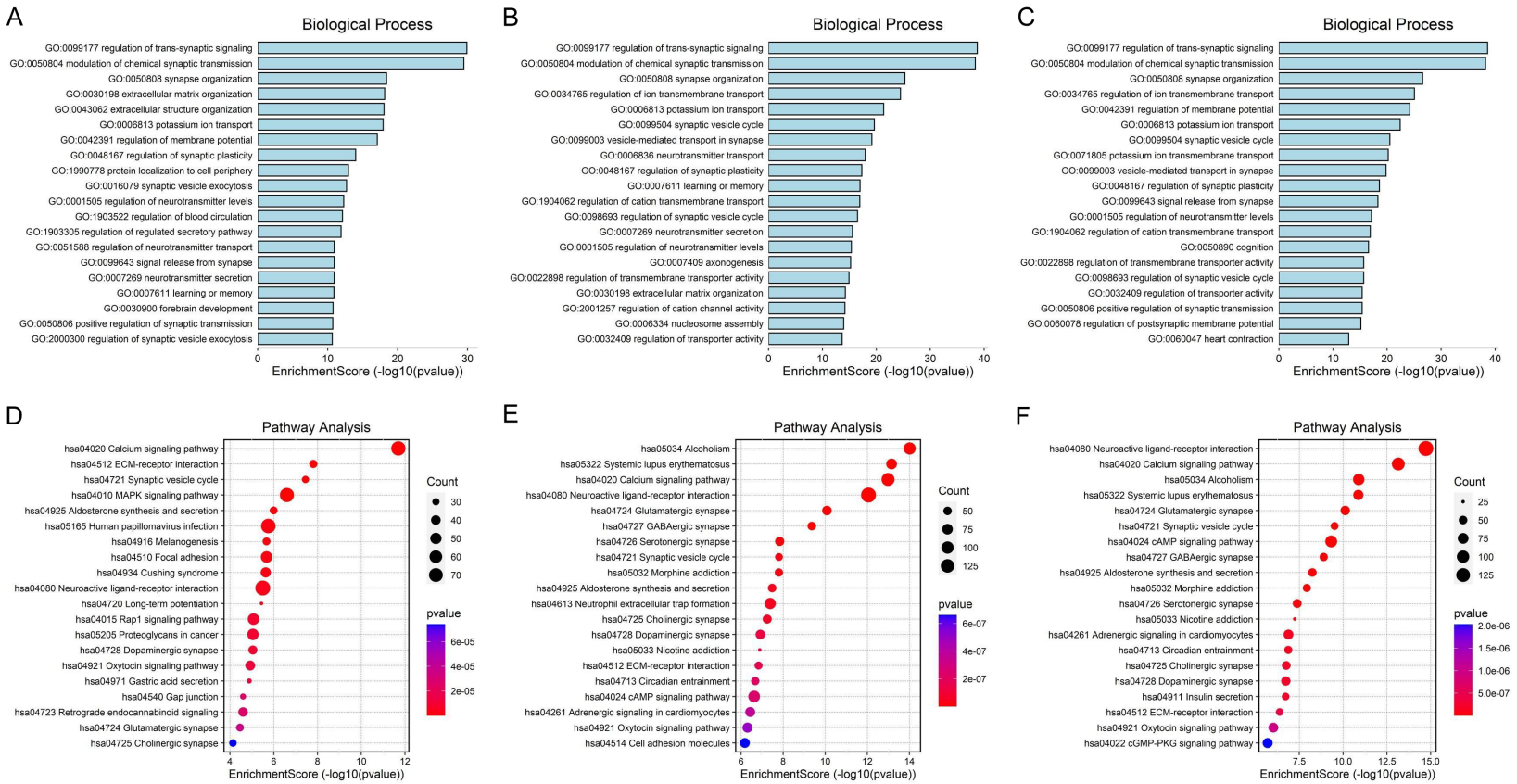

Figure 3. GO-BP and KEGG pathway enrichment analyses of target genes related to DEmiRNA, DElncRNA, and DEcircRNA. A. Top 20 enriched GO-BP terms for target genes regulated by DEmiRNA; B. Top 20 enriched GO-BP terms for target genes regulated by DElncRNA; C. Top 20 enriched GO-BP terms for target genes regulated by DEcircRNA; D. Top 20 enriched KEGG signaling pathways for target genes regulated by DEmiRNA; E. Top 20 enriched KEGG signaling pathways for target genes regulated by DElncRNA; F. Top 20 enriched KEGG signaling pathways for target genes regulated by DEcircRNA.

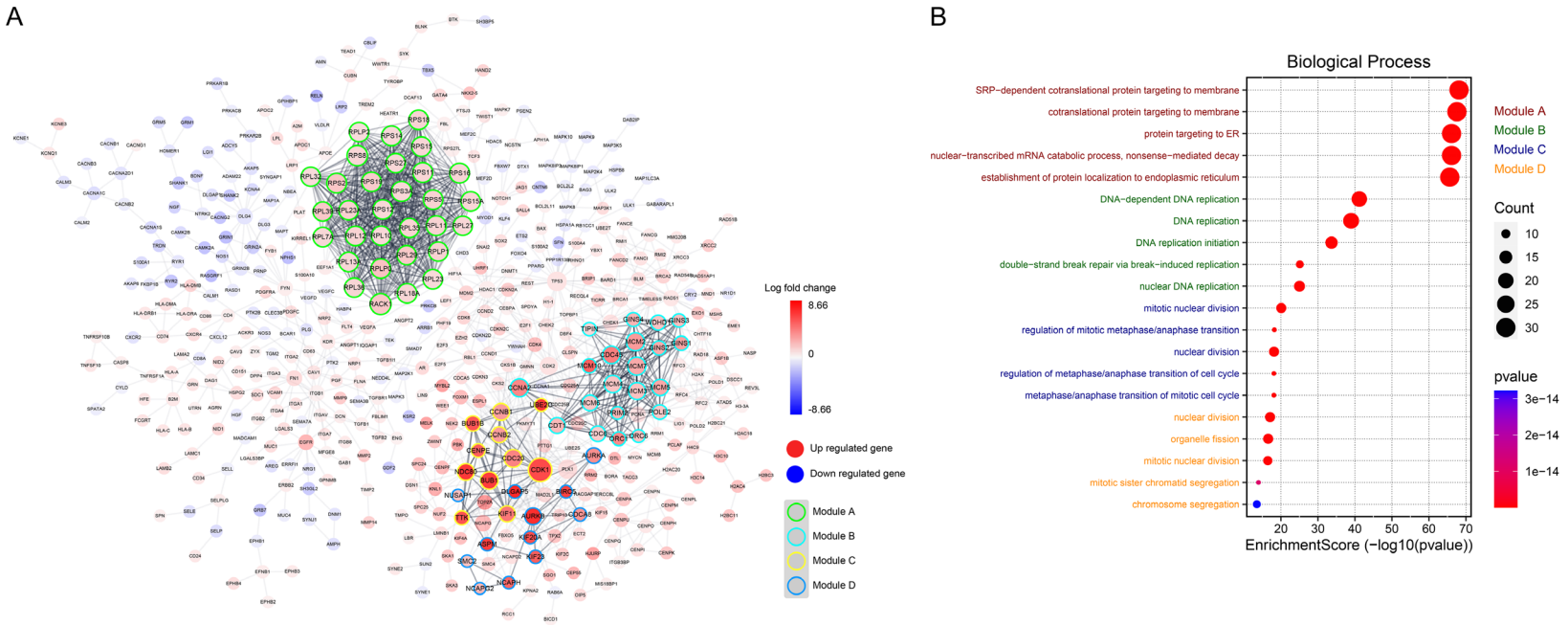

Figure 4. GO-BP enrichment analysis of genes in the PPI network and four subnetwork modules. A. PPI network constructed on the basis of three regulatory relationships: DEmiRNA-DEmRNA, DElncRNA-DEmRNA, and DEcircRNA-DEmRNA. Red indicates upregulated genes, blue indicates downregulated genes, and shades of these colors indicate fold changes in gene differential expression. A gene represents a node, and an interaction pair represents an edge. A larger node shape indicates a higher corresponding degree and a greater number of edges connected to it; B. Top 5 enriched GO-BP terms for the related genes in the four subnetwork modules.

Table 1. KEGG pathway enrichment analysis of A-D subnetwork module

Subnetwork module	Description	ID	*P*-value	Count
Module A	Ribosome	hsa03010	8.14869E-52	30
Module A	Coronavirus disease - COVID-19	hsa05171	2.18188E-46	30
Module B	Cell cycle	hsa04110	6.17304E-19	11
Module B	DNA replication	hsa03030	8.25061E-17	8
Module C	Cell cycle	hsa04110	1.45383E-12	7
Module C	Oocyte meiosis	hsa04114	5.47173E-08	5
Module C	Progesterone-mediated oocyte maturation	hsa04914	1.58473E-06	4
Module C	p53 signaling pathway	hsa04115	3.78711E-05	3
Module C	Cellular senescence	hsa04218	0.000363561	3
Module C	Human immunodeficiency virus 1 infection	hsa05170	0.000893418	3
Module C	Human T-cell leukemia virus 1 infection	hsa05166	0.001021757	3
Module C	FoxO signaling pathway	hsa04068	0.006794652	2
Module C	Ubiquitin mediated proteolysis	hsa04120	0.007945015	2
Module C	Viral carcinogenesis	hsa05203	0.015935584	2
Module D	Apoptosis - multiple species	hsa04215	0.011784803	1
Module D	Platinum drug resistance	hsa01524	0.026748288	1
Module D	Colorectal cancer	hsa05210	0.031461071	1
Module D	Progesterone-mediated oocyte maturation	hsa04914	0.037240502	1
Module D	Oocyte meiosis	hsa04114	0.047657036	1
Module D	Apoptosis	hsa04210	0.049445361	1

the aurora kinase family, such as aurora kinase B (AURKB, degree = 21) and AURKA (degree = 17).

GO-BP enrichment analysis was performed on the DEmRNAs in each subnetwork module. According to the order of importance, the first five terms of each subnetwork module GO-BP were selected and visualized by drawing a bubble chart (**Figure 4B**). The GO terms signal-recognition particle (SRP)-dependent cotranslational protein targeting to membrane (GO: 0006614) and cotranslational protein targeting to membrane (GO: 0006613) were most enriched in the genes of module A, while the terms DNA-dependent DNA replication (GO: 0006261) and DNA replication (GO: 0006260) were closely related to the genes in module B. The terms mitotic nuclear division (GO: 0140014) and regulation of the mitotic metaphase/anaphase transition (GO: 0030071) were the main terms enriched in the genes of module C, while the terms nuclear division (GO: 0000280) and organelle fission (GO: 0048285) were the main terms enriched in the genes of module C. The KEGG pathways enriched by the four subnetwork modules are all listed in **Table 1**.

Construction of the lncRNA-miRNA-mRNA ceRNA network

To better understand the interactions of DElncRNAs, DEmiRNAs, and DEmRNAs in GBM, on the basis of the regulatory relationship of DEmiRNAs-DEmRNAs and DEmiRNAs-DElncRNAs, we selected lncRNAs and mRNAs that were significantly different and were regulated by the same miRNA and then further constructed an lncRNA-miRNA-mRNA-associated ceRNA regulatory network (**Figure 5**). In this network, there were a total of 210 nodes and 204 interaction pairs, including 37 upregulated lncRNAs and 40 downregulated lncRNAs, three upregulated miRNAs and 11 downregulated miRNAs, and 55 upregulated mRNAs and 64 downregulated mRNAs.

Construction of the circRNA-miRNA-mRNA ceRNA network

According to the screening strategy described in the previous step, we integrated the regulatory relationship between DEmiRNA-DEmRNA and DEmiRNA-DEcircRNA, selected DEcircRNA and DEmRNA genes with the same miRNA response element, and constructed a circRNA-

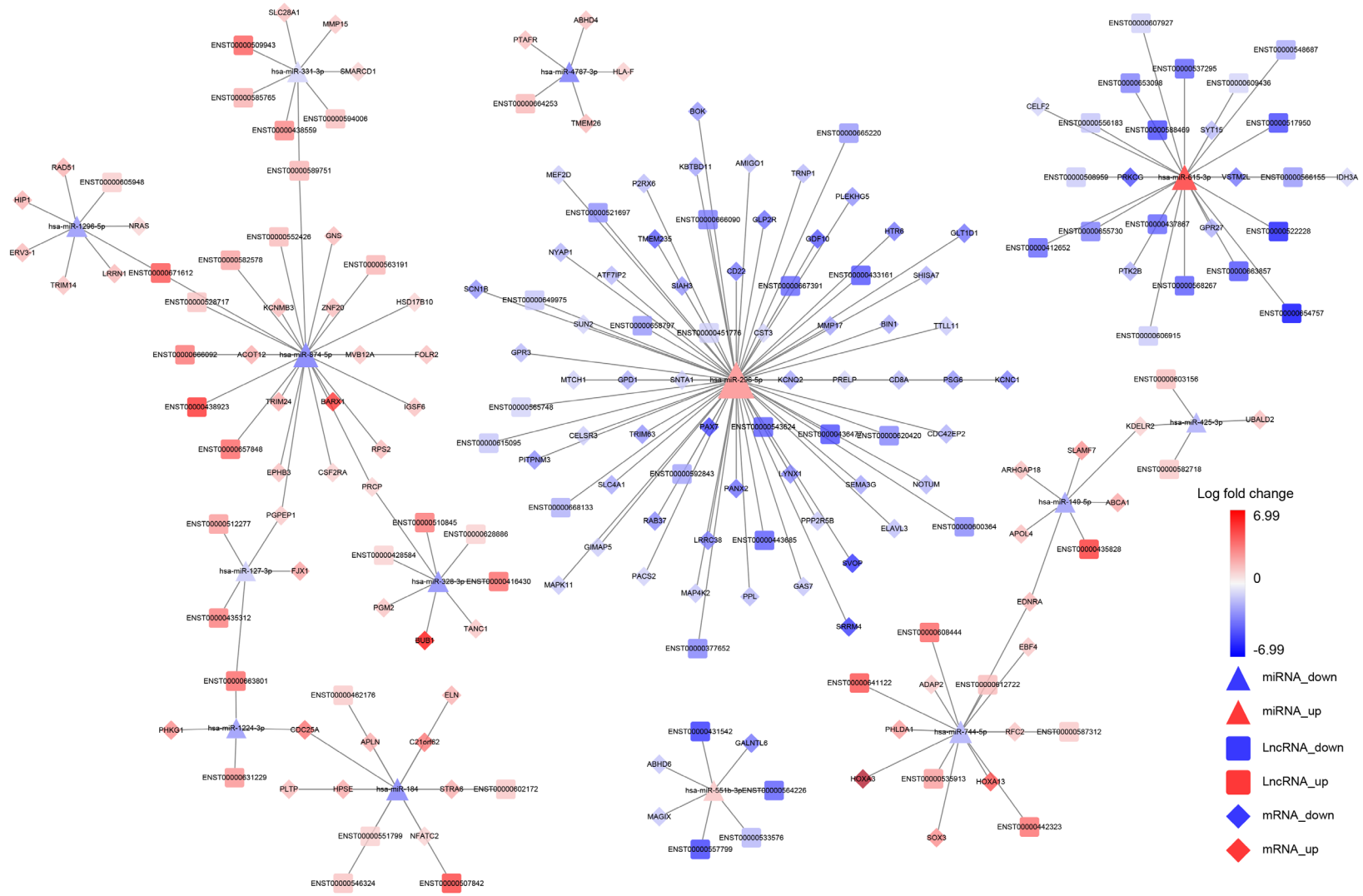

Figure 5. lncRNA-miRNA-mRNA ceRNA network. Red indicates upregulated genes, blue indicates downregulated genes, and shades of these colors indicate fold changes in gene differential expression. Triangles indicate miRNAs, squares indicate lncRNAs, and diamonds indicate mRNAs; a gene represents a node, and the line between two nodes represents an interacting pair.

miRNA-mRNA interaction network, which displayed multiple ceRNA regulatory relationships. The analysis showed that the ceRNA regulatory network in **Figure 6** had a total of 129 nodes and 126 pairs of interactions. Among them were nine upregulated circRNAs and 23 downregulated circRNAs; three upregulated miRNAs and five downregulated miRNAs; and 25 upregulated mRNAs and 64 downregulated mRNAs.

Construction of the circRNA/lncRNA-miRNA-mRNA ceRNA network

The ceRNA regulatory mechanism between ncRNAs and mRNAs is very important. circRNAs or lncRNAs can act as miRNA sponges to manipulate gene expression, thereby playing a key role in tumor development. To fully explore the key genes related to GBM and to make the ceRNA network more concise and effective, we integrated the previously constructed lncRNA-miRNA-mRNA and circRNA-miRNA-mRNA regulatory networks and then focused on screening for DEcircRNAs, DElncRNAs, and DEmRNAs regulated by the same miRNA. Based on this, a circRNA/lncRNA-miRNA-mRNA regulatory network composed of 181 nodes and 178 interacting pairs was constructed (**Figure 7**). In this more complex ceRNA network, a total of seven upregulated circRNAs and 23 downregulated circRNAs, 16 upregulated lncRNAs and 40 downregulated lncRNAs, three upregulated miRNAs (hsa-miR-296-5p, hsa-miR-615-3p, and hsa-miR-551b-3p), four downregulated miRNAs (hsa-miR-874-5p, hsa-miR-331-3p, hsa-miR-1224-3p, and hsa-miR-4787-3p), and 24 upregulated mRNAs and 64 downregulated mRNAs were identified. **Table 2** shows the seven miRNA-targeted binding mRNAs in the ceRNA network.

Verification of differential expression of mRNAs, miRNAs, lncRNAs, and circRNAs

To confirm the reliability of the results of our high-throughput RNA-Seq and the feasibility of the ceRNA regulatory network, we selected the relevant genes from the regulatory network and expanded the quantity of samples (20 sample tissues in each group) for RT-qPCR verification. In **Figure 7**, a gene represents a node, and an edge represents an interaction pair. We observed that among the upregulated miRNAs, hsa-miR-296-5p, as the central node of the network, had the most connected edges, while among the downregulated miRNAs, hsa-miR-874-5p had the most connected edges. These are likely to play a key role in the ceRNA regulatory mechanism of GBM. Therefore, we used hsa-miR-296-5p and hsa-miR-874-5p as the starting points to randomly select DEmRNAs, DElncRNAs and DEcircRNAs with the same miRNA response elements from the regulatory network. Finally, based on the circRNA/lncRNA-miRNA-mRNA regulatory relationship, we chose the hsa_circ_0139982/lncRNA-ENST00000-666090-hsa-miR-296-5p-cluster of differentiation 22 (CD22) and hsa_circ_0000350/lncRNA-ENST00000438923-hsa-miR-874-5p-tripartite motif 24 (TRIM24) signalling pathways. As shown in **Figure 8A-D**, the expression levels of hsa-miR-296-5p were significantly higher in GBM tissues, while the mRNA expression levels of lncRNA-ENST00000666090 and CD22 were significantly lower. The RT-qPCR data of hsa_circ_0139982 were inconsistent with the RNA-Seq results. We speculate that the reason for this was likely the difference in the experimental technique itself or the principle of expression level calculation. In addition, compared to normal cerebral cortical tissue, the expression level of miR-874-5p in **Figure 8E-H** was significantly lower in GBM tissues, while the expression levels hsa_circ_0000350, lncRNA-ENST00000438923, and TRIM24 were significantly higher. In summary, the RT-qPCR results were basically consistent with the RNA-Seq results, which supports the validity of the RNA-Seq data in this study.

TCGA-based GBM data validation

From the TCGA and GSE165397 datasets, the expression profiles of GBM mRNAs and GBM miRNAs were obtained. Using $P < 0.05$ and $|\log FC| > 2$ as the screening conditions and using the software limma for differential expression analysis, 7040 DEmRNAs and 221 DEmiRNAs were finally selected. In addition, the selected genes were intersected with the DEmRNA and DEmiRNA data obtained by RNA-Seq, and Venn diagrams with the same DEmRNA and DEmiRNA were produced. As shown in **Figure 9A** and **9B**, 3932 DEmRNAs were shared in common by the two groups, accounting for 3932/5289 (74.34%) of the total DEmRNAs identified by RNA-Seq; 99 identical DE miRNAs accounted for 99/259

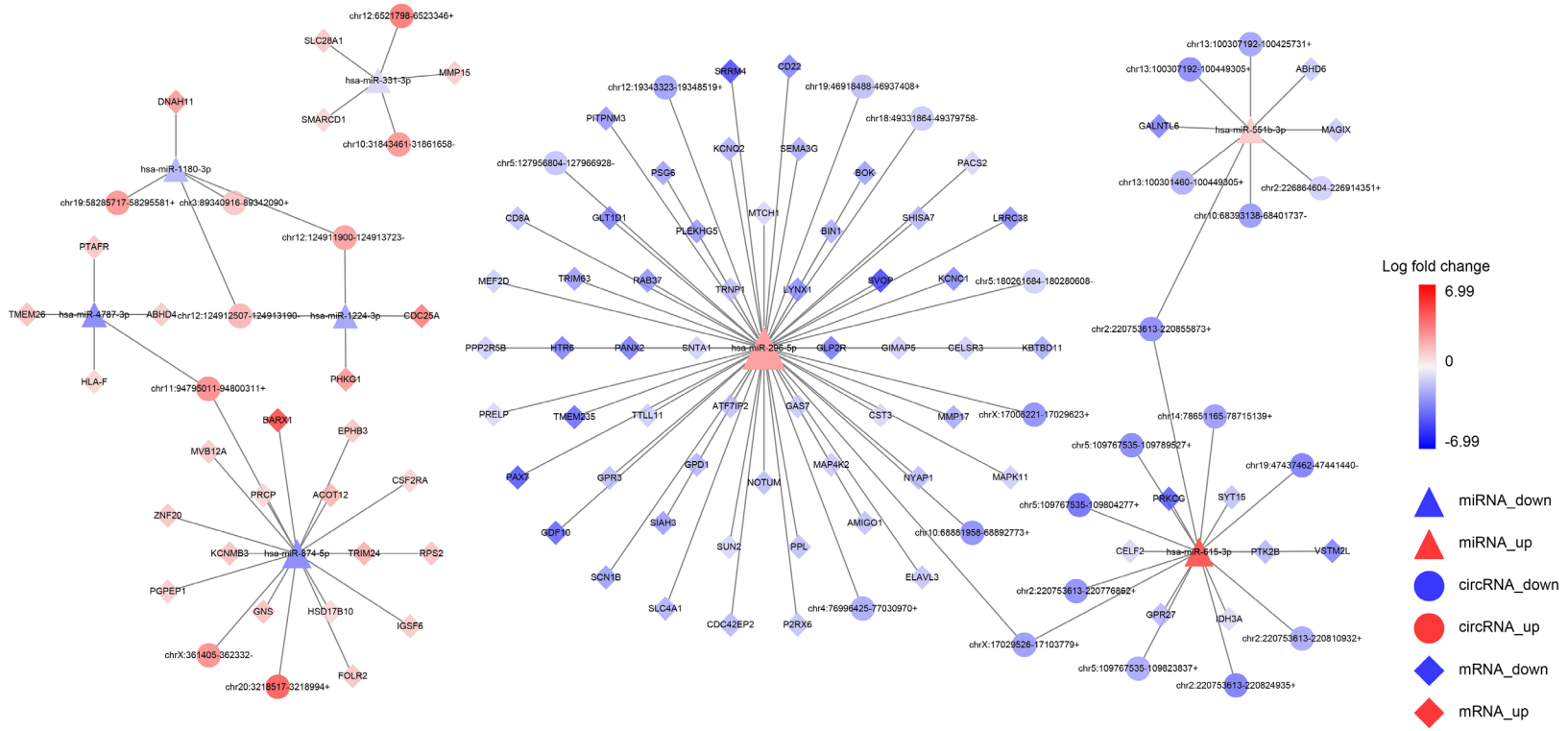

Figure 6. circRNA-miRNA-mRNA ceRNA network. Red indicates upregulated genes, blue indicates downregulated genes, and shades of these colors indicate fold changes in gene differential expression. Triangles indicate miRNAs, circles indicate circRNAs, and diamonds indicate mRNAs; a gene represents a node, and the line between two nodes represents an interacting pair.

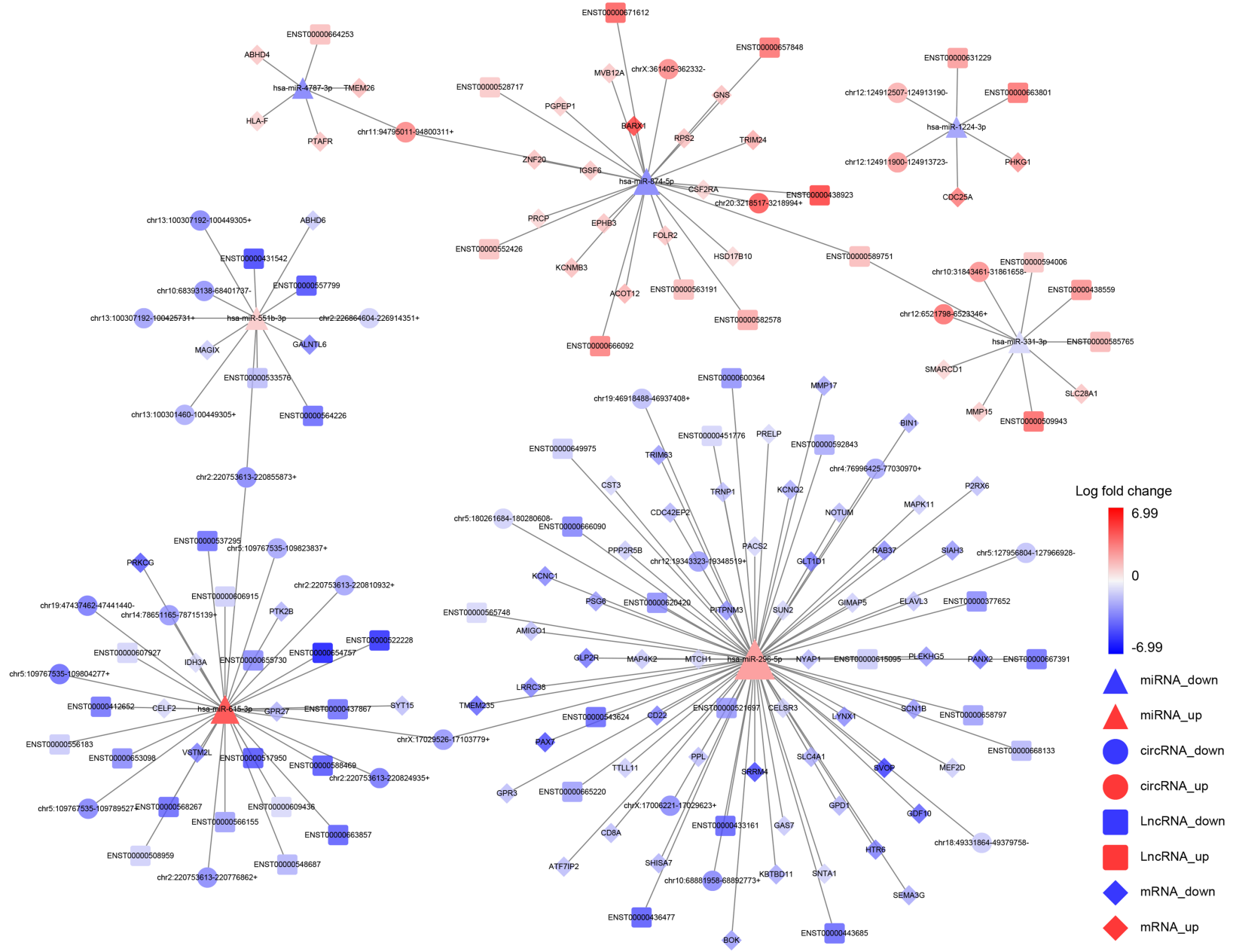
hsa-miR-4787-3p
ABHD4
ENST00000664253
TMEM26
HLA-F
PTAFR
chr11:94795011-94800311+
hsa-miR-874-5p
ENST00000671612
ENST00000657848
MVB12A
chrX:361405-362332-
ENST00000528717
GNS
PGPEP1
BARX1
RPS2
TRIM24
ZNF20
IGSF6
CSF2RA
chr20:3218517-3218994+
ENST00000438923
PRCP
EPHB3
FOLR2
HSD17B10
ENST00000552426
KCNMB3
ACOT12
ENST00000563191
ENST00000582578
ENST00000666092
ENST00000589751
hsa-miR-1224-3p
ENST00000631229
chr12:124912507-124913190-
ENST00000663801
chr12:124911900-124913723-
PHKG1
CDC25A
hsa-miR-331-3p
ENST00000594006
chr10:31843461-31861658-
ENST00000438559
chr12:6521798-6523346+
ENST00000585765
SMARCD1
SLC28A1
MMP15
ENST00000509943
hsa-miR-551b-3p
chr13:100307192-100449305+
ABHD6
ENST00000431542
chr10:68393138-68401737-
ENST00000557799
chr13:100307192-100425731+
chr2:226864604-226914351+
MAGIX
GALNTL6
ENST00000533576
chr13:100301460-100449305+
ENST00000564226
chr2:220753613-220855873+
hsa-miR-296-5p
ENST00000600364
chr19:46918488-46937408+
MMP17
ENST00000451776
PRELP
ENST00000592843
BIN1
ENST00000649975
TRIM63
chr4:76996425-77030970+
CST3
TRNP1
KCNQ2
P2RX6
CDC42EP2
NOTUM
MAPK11
chr5:180261684-180280608-
ENST00000666090
PACS2
PPP2R5B
chr12:19343323-19348519+
GLT1D1
RAB37
SIAH3
chr5:127956804-127966928-
KCNC1
PSG6
ENST00000620420
PITPNM3
SUN2
GIMAP5
ELAVL3
ENST00000377652
ENST00000565748
AMIGO1
GLP2R
MAP4K2
MTCH1
NYAP1
ENST00000615095
PLEKHG5
PANX2
ENST00000667391
LRRC38
TMEM235
ENST00000543624
CD22
ENST00000521697
CELSR3
LYNX1
SCN1B
ENST00000658797
PAX7
ENST00000668133
TTLL11
PPL
SRRM4
SLC4A1
SVOP
MEF2D
GPR3
ENST00000665220
chrX:17006221-17029623+
GPD1
GDF10
CD8A
ENST00000433161
GAS7
chr18:49331864-49379758-
HTR6
ATF7IP2
SHISA7
chr10:68881958-68892773+
KBTBD11
SNTA1
SEMA3G
ENST00000436477
BOK
ENST00000443685
chrX:17029526-17103779+
hsa-miR-645-3p
ENST00000537295
chr5:109767535-109823837+
PRKCG
ENST00000606915
chr2:220753613-220810932+
chr19:47437462-47441440-
chr14:78651165-78715139+
PTK2B
ENST00000607927
IDH3A
ENST00000655730
ENST00000654757
ENST00000522228
chr5:109767535-109804277+
ENST00000412652
CELF2
GPR27
ENST00000437867
SYT15
ENST00000556183
ENST00000653098
VSTM2L
ENST00000517950
ENST00000588469
chr2:220753613-220824935+
chr5:109767535-109789527-
ENST00000568267
ENST00000609436
ENST00000566155
ENST00000663857
ENST00000508959
ENST00000548687
chr2:220753613-220776862+
Log fold change
6.99
0
-6.99
miRNA_down
miRNA_up
circRNA_down
circRNA_up
LncRNA_down
LncRNA_up
mRNA_down
mRNA_up

Figure 7. circRNA/lncRNA-miRNA-mRNA ceRNA network. Red indicates upregulated genes, blue indicates downregulated genes, and shades of these colors indicate fold changes in gene differential expression. Triangles indicate miRNAs, circles indicate circRNAs, squares indicate lncRNAs, and diamonds indicate mRNAs; a gene represents a node, and the line between two nodes represents an interacting pair.

Table 2. Targeted binding mRNAs of seven miRNAs in ceRNA network

miRNA	Fold change	Regulation	Number of target mRNA	Gene
hsa-miR-296-5p	9.001087412	up	54	SNTA1, PANX2, PRELP, KCNC1, BOK, SCN1B, KCNQ2, TMEM235, SUN2, CELSR3, GIMAP5, MAP4K2, GAS7, ELAVL3, CDC42EP2, TTLL11, HTR6, PLEKHG5, TRNP1, AMIGO1, KBTBD11, P2RX6, NYAP1, GPR3, PITPNM3, SRRM4, GLT1D1, CD22, GPD1, RAB37, PPP2R5B, CD8A, GDF10, SIAH3, TRIM63, LRRC38, SEMA3G, BIN1, GLP2R, ATF7IP2, MTCH1, SLC4A1, PACS2, PPL, SVOP, NOTUM, PSG6, SHISA7, MEF2D, MAPK11, CST3, PAX7, LYNX1, MMP17
hsa-miR-615-3p	51.36935626	up	7	PTK2B, IDH3A, VSTM2L, CELF2, GPR27, SYT15, PRKCG
hsa-miR-551b-3p	2.900059925	up	3	MAGIX, GALNTL6, ABHD6
hsa-miR-874-5p	13.91429265	down	15	MVB12A, PGPEP1, ZNF20, PRCP, KCNMB3, ACOT12, TRIM24, BARX1, EPHB3, CSF2RA, RPS2, IGSF6, FOLR2, HSD17B10, GNS
hsa-miR-4787-3p	14.23393622	down	4	ABHD4, HLA-F, PTAFR, TMEM26
hsa-miR-331-3p	2.186596554	down	3	SMARCD1, MMP15, SLC28A1
hsa-miR-1224-3p	7.579023732	down	2	CDC25A, PHKG1

(38.22%) of the total DEmRNAs identified by RNA-Seq. The remaining different DEmRNAs and DEmiRNAs may be related to sample differences and different screening thresholds. It should be emphasized that we found that the core genes in the PPI network (RPS8, RPS3A, RPS27, MCM2, MCM7, MCM3, CDK1, CDC20, AURKB, and AURKA) were among these 3932 identical DEmRNAs; similarly, hsa-miR-296-5p and hsa-miR-874-5p, as key genes in the ceRNA network, were also among the 99 shared DEmiRNAs.

Survival analysis validation

Using the clinical data for GBM in the Chinese Glioma Genome Atlas (CGGA) database, we performed data mining and survival analysis on the DEmRNAs in the ceRNA regulatory network that could be targets of hsa-miR-296-5p and hsa-miR-874-5p according to online tools. The results showed that eight DEmRNAs were associated with the survival prognosis of patients ($P < 0.05$). Among the DEmRNAs, ion channel protein kv3.1 (KCNC1), embryonic lethal abnormal vision-like protein 3 (ELAVL3), phosphatidylinositol transfer protein 3 (PITPNM3), protein phosphatase 2, regulatory subunit B', beta (PPP2R5B) and ly6/neurotoxin 1 (LYNX1) could be complementarily paired with hsa-miR-296-5p, and their expression levels were significantly downregulated in the GBM group (**Figure 10A-E**). The results of the Kaplan-Meier curve analysis are shown in **Figure 10A-E**. The expression levels of the five target DEmRNAs that interacted with hsa-miR-296-5p were positively correlated with the overall survival rate of GBM patients ($P < 0.05$). TRIM24, BARX homeobox 1 (BARX1) and immunoglobulin superfamily 6 (IGSF6) were the target genes of hsa-miR-874-5p, and their expression levels were significantly increased in the GBM group (**Figure 10F-H** box plot). In addition, the survival analysis showed that patients with low expression of these three target genes had a longer survival time, and the expression levels of these genes were negatively correlated with the overall survival rate (**Figure 10F-H**, $P < 0.05$). Therefore, we speculate that KCNC1, ELAVL3, PITPNM3, PPP2R5B, and LYNX1 have inhibitory effects

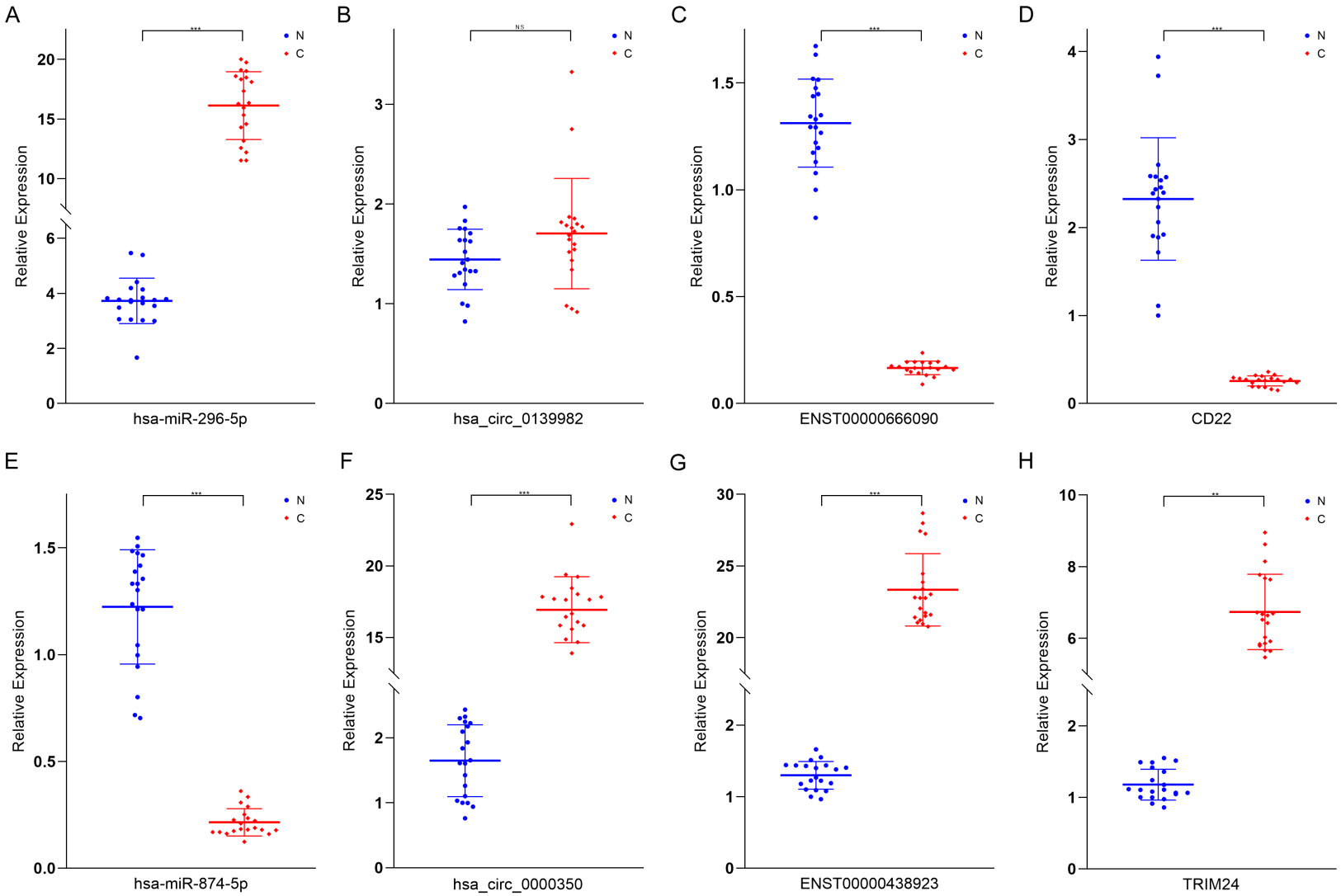

Figure 8. RT-qPCR validation of related genes in circRNA/lncRNA-miRNA-mRNA regulatory network. A-D. RT-qPCR detection of the differential expression of hsa-miR-296-5p, hsa_circ_0139982, ENST00000666090, and CD22 in group N and C samples; E-H. RT-qPCR detection of the differential expression of hsa-miR-874-5p, hsa_circ_0000350, ENST00000438923, and TRIM24 in group N and C samples. N: normal cerebral cortical tissue, C: GBM tissue. *$P < 0.05$, **$P < 0.01$, ***$P < 0.001$, NS: no significance.

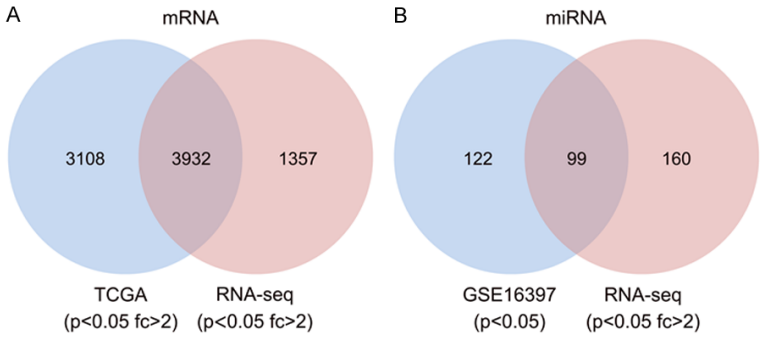

Figure 9. Venn diagram of DEmRNA and DEmiRNA. A. Venn diagram of DEmRNAs in TCGA data and sequencing data; B. Venn diagram of DEmiRNAs in GSE165397 data and sequencing data.

on the malignant progression of GBM, so their high expression could suggest a better prognosis. Meanwhile, TRIM24, BARX1, and IGSF6 promote the occurrence and progression of GBM, so their high expression may be closely related to a poor prognosis. Therefore, these identified genes may provide targets for GBM diagnosis and treatment and prognostic assessment.

Discussion

GBM is the most common and malignant primary intracranial tumor in adults and has a very poor prognosis. It has the third-highest 5-year mortality rate among systemic neoplastic diseases after pancreatic cancer and lung cancer [30]. As a particularly difficult tumor to treat in clinical practice, GBM still has a poorly understood pathogenesis. Therefore, we used high-throughput sequencing and bioinformatic techniques to analyze the differential expression profile of GBM and its ceRNA regulatory network in detail and further explored the interaction between these differentially expressed molecules and the pathogenesis of GBM as well as the formation of GBM heterogeneity from the perspective of molecular genetics.

High-throughput sequencing technology is a revolutionary change from traditional sequencing. It has the advantage of fast and accurate reading, allowing researchers to better identify the driver genes in tumors [31]. In our study, a total of 5341 DEmRNAs, 259 DEmiRNAs, 3122 DElncRNAs, and 2135 DEcircRNAs were found in GBM samples and normal cerebral cortex samples. In addition, we established the following screening criteria: All molecules that meet the threshold setting (Context+ threshold in TargetScan to -0.48, structure score threshold in miRanda to 140) are considered to be molecules that may bind to each other, and the molecular type is associated with the shape of the point, which is visually displayed using Cytascape software. We constructed two ceRNA regulatory networks related to lncRNA-miRNA-mRNA and circRNA-miRNA-mRNA. At the same time, the two regulatory networks were integrated, focusing on screening out DEcircRNAs, DElncRNAs, and DEmRNAs regulated by the same miRNA, and a circRNA/lncRNA-miRNA-mRNA composite network was re-established. Based on this, we finally determined that the oncogene hsa-miR-296-5p and the tumor suppressor gene hsa-miR-874-5p play key roles in the ceRNA complex network. Finally, we produced Venn diagrams of the sequencing data and TCGA data and selected hsa_circ_0139982/lncRNA-ENST00000666090-miR-296-5p-CD22 and hsa_circ_0000350/lncRNA-ENST00000438923-miR-874-5p-TRIM24-related regulatory pathways from the ceRNA network for RT-qPCR. We also selected DEmRNAs (KCNC1, ELAVL3, PITPNM3, PPP2R5B, LYNX1, TRIM24, BARX1, and IGSF6) that were closely related to the survival prognosis of patients from among the target genes of hsa-miR-296-5p and hsa-miR-874-5p ($P < 0.05$). The above results all indicate that our sequencing data are reliable.

Neuroglial synapses (NGSs), chemical synapses, and ion channel transporters play key roles in the malignant progression of GBM [32-34]. Venkatesh et al. found that NGSs had all the hallmark characteristics of glutamatergic chemical synapses. Neuroligin 3 (NLGN3) secreted by neurons can promote the growth and metastasis of GBM through the neuron-glioma neural circuit [35]. Monje et al. found that neuronal activity can increase the extracellular potassium ion concentration to cause tumor cell depolarization, thereby significantly promoting GBM cell proliferation [36]. Similarly, the calcium ion signals activated by neurons can enter tumor cells through α-amino-3-hydroxy-5-methyl-4-isoxazolepropionic acid receptors (AMPARs)

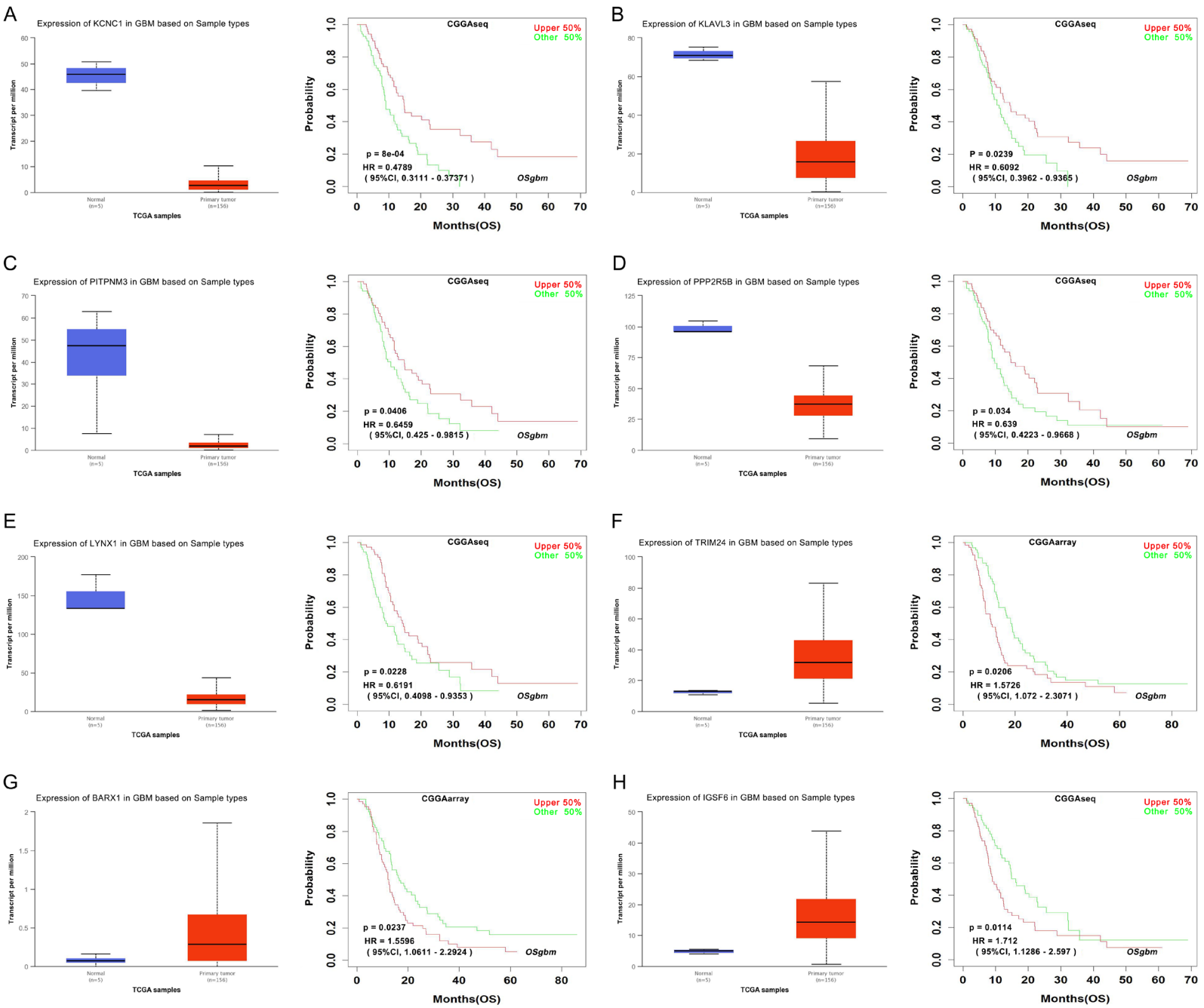
A
Expression of KCNC1 in GBM based on Sample types
Transcript per million
Normal (n=5)
Primary tumor (n=156)
TCGA samples
CGGAseq
Upper 50%
Other 50%
Probability
p = 8e-04
HR = 0.4789
(95%CI, 0.3111 - 0.37371)
OSgbm
Months(OS)
B
Expression of KLAVL3 in GBM based on Sample types
P = 0.0239
HR = 0.6092
(95%CI, 0.3962 - 0.9365)
C
Expression of PITPNM3 in GBM based on Sample types
p = 0.0406
HR = 0.6459
(95%CI, 0.425 - 0.9815)
D
Expression of PPP2R5B in GBM based on Sample types
p = 0.034
HR = 0.639
(95%CI, 0.4223 - 0.9668)
E
Expression of LYNX1 in GBM based on Sample types
p = 0.0228
HR = 0.6191
(95%CI, 0.4098 - 0.9353)
F
Expression of TRIM24 in GBM based on Sample types
CGGAarray
p = 0.0206
HR = 1.5726
(95%CI, 1.072 - 2.3071)
G
Expression of BARX1 in GBM based on Sample types
p = 0.0237
HR = 1.5596
(95%CI, 1.0611 - 2.2924)
H
Expression of IGSF6 in GBM based on Sample types
p = 0.0114
HR = 1.712
(95%CI, 1.1286 - 2.597)

Figure 10. Relationships between the expression levels of target genes and overall survival among GBM patients. A-E. Expression levels of KCNC1, ELAVL3, PITPNM3, PPP2R5B, and LYNX1 in GBM patients (n = 156) compared to normal controls (n = 5) and survival analysis; F-H. Expression levels of TRIM24, BARX1, and IGSF6 in GBM patients (n = 156) compared to normal controls (n = 5) and survival analysis. Data acquisition was based on the UALCAN online analysis tool of the TCGA and CGGA databases.

and other electrolyte ions, thereby enhancing the invasiveness of GBM cells [35, 37]. In this study, some visual results are particularly noteworthy. For example, the downregulated DEmRNAs were closely related to the modulation of chemical synaptic transmission, regulation of ion transmembrane transport, and regulation of membrane potential. Similarly, enrichment analysis based on the three regulatory relationships, DEmiRNA-DEmRNA, DElncRNA-DEmRNA, and DEcircRNA-DEmRNA, also further confirmed the direct participation of modulation of chemical synaptic transmission, regulation of ion transmembrane transport, and regulation of membrane potential in GBM cells. In view of this, we believe that these genes involved in the regulation of chemical synaptic transmission and ion channel transport may play an important role in the proliferation and invasion of GBM. An in-depth understanding of the chemical and electrophysiological activities between neurons and glioma cells can help us develop cancer drugs targeting the neuron-glioma neural circuit.

GBM cells proliferate rapidly. After disorderly evolution, they often undergo invasive growth and metastasis in the brain, making them like a "time bomb" hidden in the brain [1, 38]. More importantly, during the entire invasion and spreading process, we can often observe pathological mitosis in tumor cells [39]. Tumor treating fields (TTFs), as an innovative treatment technique, have been included in the National Comprehensive Cancer Network Central Nervous System Tumor Guidelines and the Chinese Guidelines for the Diagnosis and Treatment of Glioma [40]. GBM cells need to synthesize a large quantity of polar charged proteins and nucleic acids during the process of division and proliferation. TTF can affect these highly charged substances by generating low-field-strength (1-3 V/CM) and medium-frequency (150-200 kHz) alternating-current electric fields to hinder the formation of spindles, thereby interfering with mitosis and inducing the programmed death of tumor cells [41, 42]. In this study, we extracted four subnetwork functional modules based on the topological characteristics of the PPI network. GO-BP enrichment analysis showed that the genes of these four functional modules were closely related to biological activities such as protein cotranslational translocation, DNA replication, mitotic regulation, and nuclear fission. In addition, 10 genes, including those encoding ribosomal proteins, minichromosome maintenance proteins, cyclins and aurora kinase proteins (such as RPS8, RPS3A, RPS27, MCM2, MCM7, MCM4, CDK1, CDC20, AURKB, and AURKA), were identified as the core proteins of the PPI network. They all play regulatory roles in the mitosis of GBM cells. In summary, the above evidence shows that core genes are closely associated with tumor mitosis. We speculate that these core genes may play a key role in the pathogenesis of GBM and may provide specific diagnostic and therapeutic targets for the electric-field treatment of GBM.

In recent years, as miRNA research has advanced, much evidence has shown that miR-296-5p and miR-874-5p can participate in the regulation of a variety of tumors with different regulatory effects in different types of tumors. Yan et al. found that miR-296-5p can act as a tumor suppressor to inhibit the proliferation of colorectal cancer cells through targeted binding to high mobility group AT-Hook 1 (HMGA1) and induce cell cycle arrest and apoptosis [43]. However, some studies have shown that miR-296-5p is highly expressed in pancreatic cancer tissues and cell lines, where it can bind to box mRNA and promote tumor cell invasion and drug resistance by inducing epithelial-mesenchymal transition, ultimately leading to poor prognosis [44]. In addition, miR-296-5p played a key role in the ceRNA regulatory network. Overexpression of circPSMC3 can regulate PTEN in cells by downregulating the expression of miR-296-5p and can ultimately inhibit the proliferation and metastasis of gastric cancer cells [45]. Similar conclusions have been reached in studies related to miR-874-5p. Studies have shown that miR-874-5p can be used as a tumor suppressor to inhibit the mevalonate

pathway by targeting sterol regulatory element-binding factor-2 (SREBF2) and phosphomevalonate kinase (PMVK), thereby inducing apoptosis or cycle arrest in breast cancer cells [46]. Similarly, reduced expression of miR-874-5p was detected in paclitaxel-resistant ovarian cancer cell lines. Further research has demonstrated that overexpressed miR-874-5p can target 3'-untranslated regions (3'-UTR) binding to salt-inducible kinase 2 (SIK2) to inhibit tumor cell proliferation, thereby enhancing the cytotoxicity of paclitaxel [47]. Some new evidence suggests that circRNAs can act as regulators of apoptosis to mediate the occurrence and development of cancer. For example, circ_0003340 can act as a "molecular sponge" as a ceRNA molecule, inhibiting cell apoptosis by adsorbing miR-874-5p/enabled homologue (ENAH), thereby promoting malignant progression and chemoresistance of esophageal cancer [48]. In addition, circ_0001588 overexpression can significantly promote the proliferation, migration, and invasion of liver cancer cells and is induced by the antagonistic effect of miR-874-5p [49]. In this study, we found that hsa-miR-296-5p and hsa-miR-874-5p were located in the center of the ceRNA regulatory network as marker molecules. In addition, based on the information in the CGGA database, we used univariate survival analysis to investigate the effect of DEmRNAs that bound to hsa-miR-296-5p and hsa-miR-874-5p in the ceRNA regulatory network on the survival and prognosis of GBM patients. Eight molecules (KCNC1, ELAVL3, PITPNM3, PPP2R5B, LYNX1, TRIM24, BARX1, and IGSF6) had significant effects on GBM survival ($P < 0.05$). We speculate that there is a close correlation between hsa-miR-296-5p and hsa-miR-874-5p and the pathogenesis and prognostic assessment of GBM, and they may be potential key miRNAs for GBM targeted therapy. In addition, although the results of this study have some significance, there are 'a few limitations. First, due to the small sample size in this study, there may have been deviations in the screening results during the difference analysis. Therefore, it is necessary to continue to expand the sample size and improve the research content. Second, the functions of the identified DEmiRNAs have not been thoroughly explored. In future studies, the predicted circRNA/lncRNA-miRNA-mRNA regulatory network needs to be further confirmed through cell function experiments and animal models to elucidate its exact regulatory function and molecular mechanism in GBM. Third, this study is limited to exploring the impact of ceRNA network regulation on the pathogenesis of GBM. However, relevant studies have shown that the impact of ncRNA on disease is not only through the above mechanisms, but also through binding to functional proteins, translating important polypeptides, and other ways to play important roles. Therefore, other modes of action in circRNA/lncRNA need to be further discussed.

Conclusion

This study explored the molecular mechanism of GBM based on full transcriptome sequencing and experimental validation. Screening out hub genes involved in tumor mitosis may play an important role in GBM malignant progression. In addition, we constructed a ceRNA regulatory network of circRNA/lncRNA-miRNA-mRNA and identified hsa-miR-296-5p and hsa-miR-874-5p as key molecules that also play a key role in the pathogenesis and prognostic evaluation of GBM. In summary, these findings not only reveal the complexity of the GBM genome but also provide evidence for the search for relevant new epigenetic markers and further clarify that ncRNA-mediated precision medicine may be an ideal treatment strategy to overcome the bottleneck in GBM treatment in the future.

Acknowledgements

We specially thank Dr. Lin Zeng (BioDataStidio in Shanghai) for sequencing data analysis. The present study was financially supported by grants from the National Natural Science Foundation of China (No: 81930091, 8177-3462, 81973077, 21805197); Post-Graduate's Innovation Fund Project of Hebei Province (No: CXZZBS2022015); Government-funded Clinical Medicine Outstanding Talent Training Project (No: 360017); Medical Science Foundation of Hebei University (No: 2020A11); Foundation Project of Affiliated Hospital of Hebei University (No: 2019Z003); and Seed Foundation of Zhejiang Provincial People's Hospital (No: ZRY2022J003).

Written informed consent was received from all participants (No. HDFY-LL-2022-046).

Disclosure of conflict of interest

None.

Address correspondence to: Dr. Zhi-Wei Sun, Department of Surgery, School of Clinical Medicine, Hebei University, Baoding 071000, Hebei, PR China. E-mail: zwsun@ccmu.edu.cn; Dr. Yu-Hao Zhang, Cancer Center, Department of Neurosurgery, Zhejiang Provincial People's Hospital, Affiliated to Hangzhou Medical College, Hangzhou 310000, Zhejiang, PR China. E-mail: zyhazzy@163.com; Dr. Ke-Bin Zheng, Department of Neurosurgery, Affiliated Hospital of Hebei University, Baoding 071000, Hebei, PR China. E-mail: zhengkebinzkb@163.com

References

[1] Lauko A, Lo A, Ahluwalia MS and Lathia JD. Cancer cell heterogeneity & plasticity in glioblastoma and brain tumors. Semin Cancer Biol 2022; 82: 162-175.

[2] Kondo T. Glioblastoma-initiating cell heterogeneity generated by the cell-of-origin, genetic/epigenetic mutation and microenvironment. Semin Cancer Biol 2022; 82: 176-183.

[3] Liang R, Wu C, Liu S and Zhao W. Targeting interleukin-13 receptor α2 (IL-13Rα2) for glioblastoma therapy with surface functionalized nanocarriers. Drug Deliv 2022; 29: 1620-1630.

[4] Petrosyan E, Fares J, Cordero A, Rashidi A, Arrieta VA, Kanojia D and Lesniak MS. Repurposing autophagy regulators in brain tumors. Int J Cancer 2022; 151: 167-180.

[5] Iannello A, Ciarrocchi A, Fragliasso V and Vaisitti T. Lift the curtain on long non-coding RNAs in hematological malignancies: pathogenic elements and potential targets. Cancer Lett 2022; 536: 215645.

[6] Zeng Z, Chen Y, Geng X, Zhang Y, Wen X, Yan Q, Wang T, Ling C, Xu Y, Duan J, Zheng K and Sun Z. NcRNAs: multi-angle participation in the regulation of glioma chemotherapy resistance (Review). Int J Oncol 2022; 60: 76.

[7] Zheng K, Xie H, Wu W, Wen X, Zeng Z and Shi Y. CircRNA PIP5K1A promotes the progression of glioma through upregulation of the TCF12/PI3K/AKT pathway by sponging miR-515-5p. Cancer Cell Int 2021; 21: 27.

[8] Zhang Y, Lin X, Geng X, Shi L, Li Q, Liu F, Fang C and Wang H. Advances in circular RNAs and their role in glioma (Review). Int J Oncol 2020; 57: 67-79.

[9] Kishore C and Karunagaran D. Non-coding RNAs as emerging regulators and biomarkers in colorectal cancer. Mol Cell Biochem 2022; 477: 1817-1828.

[10] Wang H, Meng Q, Qian J, Li M, Gu C and Yang Y. Review: RNA-based diagnostic markers discovery and therapeutic targets development in cancer. Pharmacol Ther 2022; 234: 108123.

[11] Shigematsu M and Kirino Y. Making invisible RNA visible: discriminative sequencing methods for rna molecules with specific terminal formations. Biomolecules 2022; 12: 611.

[12] Hosseini K, Ranjbar M, Pirpour Tazehkand A, Asgharian P, Montazersaheb S, Tarhriz V and Ghasemnejad T. Evaluation of exosomal noncoding RNAs in cancer using high-throughput sequencing. J Transl Med 2022; 20: 30.

[13] Wang Y, Zhou G, Guan T, Wang Y, Xuan C, Ding T and Gao J. A network-based matrix factorization framework for ceRNA co-modules recognition of cancer genomic data. Brief Bioinform 2022; 23: bbac154.

[14] Lin W, Liu H, Tang Y, Wei Y, Wei W, Zhang L and Chen J. The development and controversy of competitive endogenous RNA hypothesis in non-coding genes. Mol Cell Biochem 2021; 476: 109-123.

[15] Liu Y, Khan S, Li L, Ten Hagen TLM and Falahati M. Molecular mechanisms of thyroid cancer: a competing endogenous RNA (ceRNA) point of view. Biomed Pharmacother 2022; 146: 112251.

[16] Chen S, Zhou Y, Chen Y and Gu J. fastp: an ultra-fast all-in-one FASTQ preprocessor. Bioinformatics 2018; 34: i884-i890.

[17] Dobin A, Davis CA, Schlesinger F, Drenkow J, Zaleski C, Jha S, Batut P, Chaisson M and Gingeras TR. STAR: ultrafast universal RNA-seq aligner. Bioinformatics 2013; 29: 15-21.

[18] Liao Y, Smyth GK and Shi W. featureCounts: an efficient general purpose program for assigning sequence reads to genomic features. Bioinformatics 2014; 30: 923-930.

[19] Anders S, Pyl PT and Huber W. HTSeq--a Python framework to work with high-throughput sequencing data. Bioinformatics 2015; 31: 166-169.

[20] Cheng J, Metge F and Dieterich C. Specific identification and quantification of circular RNAs from sequencing data. Bioinformatics 2016; 32: 1094-1096.

[21] Love MI, Huber W and Anders S. Moderated estimation of fold change and dispersion for RNA-seq data with DESeq2. Genome Biol 2014; 15: 550.

[22] Yu G, Wang LG, Han Y and He QY. clusterProfiler: an R package for comparing biological themes among gene clusters. OMICS 2012; 16: 284-287.

[23] Shen S, Park JW, Lu ZX, Lin L, Henry MD, Wu YN, Zhou Q and Xing Y. rMATS: robust and flexible detection of differential alternative splic-

ing from replicate RNA-Seq data. Proc Natl Acad Sci U S A 2014; 111: E5593-5601.
[24] Friedländer MR, Mackowiak SD, Li N, Chen W and Rajewsky N. miRDeep2 accurately identifies known and hundreds of novel microRNA genes in seven animal clades. Nucleic Acids Res 2012; 40: 37-52.
[25] Szklarczyk D, Gable AL, Lyon D, Junge A, Wyder S, Huerta-Cepas J, Simonovic M, Doncheva NT, Morris JH, Bork P, Jensen LJ and Mering CV. STRING v11: protein-protein association networks with increased coverage, supporting functional discovery in genome-wide experimental datasets. Nucleic Acids Res 2019; 47: D607-D613.
[26] Shannon P, Markiel A, Ozier O, Baliga NS, Wang JT, Ramage D, Amin N, Schwikowski B and Ideker T. Cytoscape: a software environment for integrated models of biomolecular interaction networks. Genome Res 2003; 13: 2498-2504.
[27] Bader GD and Hogue CW. An automated method for finding molecular complexes in large protein interaction networks. BMC Bioinformatics 2003; 4: 2.
[28] Enright AJ, John B, Gaul U, Tuschl T, Sander C and Marks DS. MicroRNA targets in Drosophila. Genome Biol 2003; 5: R1.
[29] Agarwal V, Bell GW, Nam JW and Bartel DP. Predicting effective microRNA target sites in mammalian mRNAs. Elife 2015; 4: e05005.
[30] McBain C, Lawrie TA, Rogozińska E, Kernohan A, Robinson T and Jefferies S. Treatment options for progression or recurrence of glioblastoma: a network meta-analysis. Cochrane Database Syst Rev 2021; 5: CD013579.
[31] Napoli GC, Chau CH and Figg WD. Single whole genome sequencing analysis blazes the trail for precision medicine. Cancer Biol Ther 2022; 23: 134-135.
[32] Barria A. Dangerous liaisons as tumour cells form synapses with neurons. Nature 2019; 573: 499-501.
[33] Venkataramani V, Tanev DI, Kuner T, Wick W and Winkler F. Synaptic input to brain tumors: clinical implications. Neuro Oncol 2021; 23: 23-33.
[34] Song S, Luo L, Sun B and Sun D. Roles of glial ion transporters in brain diseases. Glia 2020; 68: 472-494.
[35] Venkatesh HS, Morishita W, Geraghty AC, Silverbush D, Gillespie SM, Arzt M, Tam LT, Espenel C, Ponnuswami A, Ni L, Woo PJ, Taylor KR, Agarwal A, Regev A, Brang D, Vogel H, Hervey-Jumper S, Bergles DE, Suvà ML, Malenka RC and Monje M. Electrical and synaptic integration of glioma into neural circuits. Nature 2019; 573: 539-545.
[36] Monje M. Synaptic communication in brain cancer. Cancer Res 2020; 80: 2979-2982.
[37] Venkataramani V, Tanev DI, Strahle C, Studier-Fischer A, Fankhauser L, Kessler T, Körber C, Kardorff M, Ratliff M, Xie R, Horstmann H, Messer M, Paik SP, Knabbe J, Sahm F, Kurz FT, Acikgöz AA, Herrmannsdörfer F, Agarwal A, Bergles DE, Chalmers A, Miletic H, Turcan S, Mawrin C, Hänggi D, Liu HK, Wick W, Winkler F and Kuner T. Glutamatergic synaptic input to glioma cells drives brain tumour progression. Nature 2019; 573: 532-538.
[38] Comba A, Faisal SM, Varela ML, Hollon T, Al-Holou WN, Umemura Y, Nunez FJ, Motsch S, Castro MG and Lowenstein PR. Uncovering spatiotemporal heterogeneity of high-grade gliomas: from disease biology to therapeutic implications. Front Oncol 2021; 11: 703764.
[39] Di Bari M, Tombolillo V, Alessandrini F, Guerriero C, Fiore M, Asteriti IA, Castigli E, Sciaccaluga M, Guarguaglini G, Degrassi F and Tata AM. M2 muscarinic receptor activation impairs mitotic progression and bipolar mitotic spindle formation in human glioblastoma cell lines. Cells 2021; 10: 1727.
[40] Rasheed S, Rehman K and Akash MSH. An insight into the risk factors of brain tumors and their therapeutic interventions. Biomed Pharmacother 2021; 143: 112119.
[41] Chen D, Le SB, Hutchinson TE, Calinescu AA, Sebastian M, Jin D, Liu T, Ghiaseddin A, Rahman M and Tran DD. Tumor treating fields dually activate STING and AIM2 inflammasomes to induce adjuvant immunity in glioblastoma. J Clin Invest 2022; 132: e149258.
[42] Hong P, Kudulaiti N, Wu S, Nie J and Zhuang D. Tumor treating fields: a comprehensive overview of the underlying molecular mechanism. Expert Rev Mol Diagn 2022; 22: 19-28.
[43] Yan G, Yan S, Wang J, Lei S, Tian W, Yue X and Zhang Y. MicroRNA-296-5p inhibits cell proliferation by targeting HMGA1 in colorectal cancer. Exp Ther Med 2021; 22: 793.
[44] Okazaki J, Tanahashi T, Sato Y, Miyoshi J, Nakagawa T, Kimura T, Miyamoto H, Fujino Y, Nakamura F, Takehara M, Ma B, Bando M, Kitamura S, Okamoto K, Muguruma N, Sogabe M and Takayama T. MicroRNA-296-5p promotes cell invasion and drug resistance by targeting Bcl2-related ovarian killer, leading to a poor prognosis in pancreatic cancer. Digestion 2020; 101: 794-806.
[45] Rong D, Lu C, Zhang B, Fu K, Zhao S, Tang W and Cao H. Correction to: CircPSMC3 suppresses the proliferation and metastasis of gastric cancer by acting as a competitive endogenous RNA through sponging miR-296-5p. Mol Cancer 2020; 19: 140.

[46] Aersilan A, Hashimoto N, Yamagata K, Yokoyama M, Nakayama A, Shi X, Nagano H, Sakuma I, Nohata N, Kinoshita T, Seki N, Rahmutulla B, Kaneda A, Zhahara SN, Gong Y, Nishimura M, Kawauchi S, Kawakami E and Tanaka T. MicroRNA-874 targets phosphomevalonate kinase and inhibits cancer cell growth via the mevalonate pathway. Sci Rep 2022; 12: 18443.

[47] Xia B, Lin M, Dong W, Chen H, Li B, Zhang X, Hou Y and Lou G. Upregulation of miR-874-3p and miR-874-5p inhibits epithelial ovarian cancer malignancy via SIK2. J Biochem Mol Toxicol 2018; 32: e22168.

[48] Wang J, Zhao N, Peng S and Zhang T. Circ_0003340 regulates the expression of ENAH to affect the development of esophageal cancer through miR-874-3p. Thorac Cancer 2023; 14: 815-826.

[49] Bin X, Chen Y, Ma J, Tang R, Zhao Z, Wang K and Wang J. circ_0001588 induces the malignant progression of hepatocellular carcinoma by modulating miR-874/CDK4 signaling. J Immunol Res 2021; 2021: 3759879.

Table S1. Clinical information for patients in this study

Patient	Age (y)	Gender	Cutting position	WHO grade	IDH typing
C1	68	Male	Right temporal lobe	WHO 4	IDH wild type (-)
C2	39	Female	Right temporal lobe	WHO 4	IDH wild type (-)
C3	45	Female	Right frontal lobe	WHO 4	IDH wild type (-)
C4	65	Male	Right frontal lobe	WHO 4	IDH wild type (-)
C5	62	Female	Right frontotemporal lobe	WHO 4	IDH wild type (-)
N1	57	Female	Right frontal lobe	-	-
N2	73	Female	Right temporal lobe	-	-
N3	40	Female	Right frontotemporal lobe	-	-
N4	56	Male	Right temporal parietal lobe	-	-
N5	36	Female	Right temporal lobe	-	-

Table S2. Primers used for RT-qPCR of differently expressed ncRNAs and mRNAs

Gene	Forward and reverse primer
hsa_circ_0139982	F: 5' TTATGAAGCTAGGCAGCCCC 3'
	R: 5' CGCTTTGCACCACACAGTTC 3'
hsa_circ_0000350	F: 5' CTCCACGAGATGGTCAAGCC 3'
	R: 5' GGACAGGACTACTGGGGCTAT 3'
lncRNA-ENST00000666090	F: 5' TGCCAGTGGATTGCTGATGT 3'
	R: 5' CAGGGTGTCAGACAAGGCTC 3'
lncRNA-ENST00000438923	F: 5' GTTTCTGGCCCCACAGTTCTA 3'
	R: 5' GCCACTTCTTCTTAAACCTGCC 3'
hsa-miR-296-5p	F: 5' GGGAGGGCCCCCCCTCAA 3'
	R: 5' CAGTGCGTGTCGTGGAGT 3'
hsa-miR-874-5p	F: 5' GGGCGGCCCCACGCACCAGG 3'
	R: 5' CAGTGCGTGTCGTGGAGT 3'
CD22	F: 5' GCACCCTGAAACCCTCTACG 3'
	R: 5' ATCAAACTTCGAGGTGTTCTTGT 3'
TRIM24	F: 5' CAGCCACAAATGCCTAAGCAG 3'
	R: 5' GTGTTGGGAACTTGGATAACTGG 3'
U6	F: 5' CTCGCTTCGGCAGCACA 3'
	R: 5' AACGCTTCACGAATTTGCG 3'
GAPDH	F: 5' GCACCGTCAAGGCTGAGAAC 3'
	R: 5' TGGTGAAGACGCCAGTGGA 3'

Table S3. The ten most significantly up and down regulated mRNAs

Gene name	Genomic position	Regulation	Fold change	*P*-value
HOXD10	chr2:176108790-176119937	up	1075.158653	1.63484E-15
HOXD9	chr2:176122719-176124937	up	660.3774172	6.40196E-19
H3C8	chr6:26269405-26271815	up	519.1851412	2.50308E-69
HOXA5	chr7:27141052-27143681	up	416.0832331	0.000106962
TOP2A	chr17:40388525-40417896	up	404.1700366	1.56542E-57
H3C12	chr6:27890315-27893106	up	320.0347284	1.91033E-32
MKI67	chr10:128096659-128126423	up	309.8003432	1.02369E-49
HOXD13	chr2:176092721-176095944	up	297.8532863	5.21752E-09
H3C2	chr6:26031589-26032099	up	297.4077971	1.04726E-59
MYBL2	chr20:43667019-43716495	up	270.3938023	3.65127E-53
NPAS4	chr11:66421004-66426707	down	926.3432834	2.11796E-23
EGR4	chr2:73290929-73293701	down	259.7143534	6.67774E-20
DAO	chr12:108858932-108901043	down	164.2756455	4.50391E-11
OPALIN	chr10:96343221-96359365	down	139.0538161	8.53526E-12
ACP7	chr19:39083913-39111493	down	136.8621909	6.47792E-13
ANKRD34C	chr15:79282722-79298239	down	125.6272434	3.56267E-18
GJB6	chr13:20221962-20232365	down	116.3568258	4.38483E-10
MOBP	chr3:39467198-39529479	down	108.3198487	1.45161E-22
OR2L8	chr1:247948858-247949796	down	108.0048627	5.57324E-09
GABRG1	chr4:46035769-46124054	down	99.21118014	6.50703E-13

Table S4. The ten most significantly up and down regulated miRNAs

Gene name	Mature sequence	Regulation	Fold change	*P*-value
hsa-miR-10b-5p	UACCCUGUAGAACCGAAUUUGUG	up	824.17332	8.2273E-23
hsa-miR-10b-3p	ACAGAUUCGAUUCUAGGGGAAU	up	631.30175	8.5466E-15
hsa-miR-196a-5p	UAGGUAGUUUCAUGUUGUUGGG	up	344.28778	1.7066E-16
hsa-miR-1246	AAUGGAUUUUUGGAGCAGG	up	205.10731	4.8725E-08
hsa-miR-novel-chrX_28811	AUGGAUUUUUGGAGCAGGGA	up	196.09056	1.3454E-12
hsa-miR-novel-chrY_29589	AUGGAUUUUUGGAGCAGGGA	up	196.09056	1.3454E-12
hsa-miR-450b-5p	UUUUGCAAUAUGUUCCUGAAUA	up	88.084399	1.0127E-05
hsa-miR-196b-5p	UAGGUAGUUUCCUGUUGUUGGG	up	72.599621	0.00023511
hsa-miR-561-5p	AUCAAGGAUCUUAAACUUUGCC	up	67.442920	0.04522225
hsa-miR-503-3p	GGGGUAUUGUUUCCGCUGCCAGG	up	57.285482	0.00015492
hsa-miR-873-3p	GGAGACUGAUGAGUUCCCGGGA	down	213.42446	8.8399E-12
hsa-miR-218-2-3p	CAUGGUUCUGUCAAGCACCGCG	down	87.353690	3.4656E-08
hsa-miR-4446-3p	CAGGGCUGGCAGUGACAUGGGU	down	78.725566	5.0666E-07
hsa-miR-873-5p	GCAGGAACUUGUGAGUCUCCU	down	69.332493	1.1611E-15
hsa-miR-219a-5p	UGAUUGUCCAAACGCAAUUCU	down	51.285003	1.9390E-05
hsa-miR-3059-3p	CCUCUAGGGAAGAGAAGGUUGG	down	38.942058	0.00017029
hsa-miR-129-1-3p	AAGCCCUUACCCCAAAAAGUAU	down	33.874207	7.8377E-12
hsa-miR-6764-5p	UCCCAGGGUCUGGUCAGAGUUG	down	30.581485	0.00065321
hsa-miR-219a-2-3p	AGAAUUGUGGCUGGACAUCUGU	down	29.941344	7.2928E-11
hsa-miR-1224-5p	GUGAGGACUCGGGAGGUGG	down	29.039332	5.3721E-06

Table S5. The ten most significantly up and down regulated lncRNAs

Transcript ID	Genomic position	Regulation	Fold change	*P*-value
ENST00000440016	chr2:176121611-176137013	up	796.530975	6.08412E-18
ENST00000464382	chr17:48557262-48560333	up	545.565294	0.002667198
ENST00000655443	chr2:91759462-91767701	up	482.227213	4.19416E-14
ENST00000524304	chr7:27150052-27152726	up	384.060433	0.000167283
ENST00000443966	chr20:58826736-58840844	up	346.998291	3.12975E-34
ENST00000519935	chr7:27168899-27171915	up	240.430296	0.008989083
ENST00000605044	chr20:58876592-58876981	up	222.583008	2.64382E-11
ENST00000518088	chr7:27107777-27122173	up	198.202748	0.00039980
ENST00000518947	chr7:27147163-27155928	up	197.646201	0.00057512
ENST00000608941	chr2:176164164-176165716	up	185.485875	1.31131E-09
ENST00000501520	chr16:28284885-28292064	down	724.941647	3.37636E-15
ENST00000581719	chr18:902766-906667	down	393.193409	1.48791E-05
ENST00000657482	chr12:110936583-11095796	down	212.362281	1.01551E-10
ENST00000502515	chr5:177782197-177794396	down	184.589888	8.12238E-12
ENST00000507304	chr5:169013264-169024987	down	169.530341	1.36797E-12
ENST00000667122	chr6:170088077-170093059	down	158.764152	0.014527503
ENST00000671665	chr7:155067034-155072450	down	152.378677	1.09836E-09
ENST00000654089	chr11:7434097-7513628	down	151.792399	6.94685E-10
ENST00000633012	chr1:230426491-230436822	down	146.073670	8.42719E-07
ENST00000521048	chr8:119223804-119246843	down	144.008454	3.53741E-13

Table S6. The ten most significantly up and down regulated circRNAs

circBaseID	Genomic position	Regulation	Fold change	*P*-value
hsa_circ_0000992	chr2:37316237-37317179	up	93.9360595	8.94427E-09
novel_circRNA	chr13:110192829-110198597	up	77.7356709	8.38596E-07
hsa_circ_0069399	chr4:36228582-36229645	up	61.9194807	3.76511E-06
hsa_circ_0012389	chr1:48451552-48453131	up	61.8226229	8.87228E-07
hsa_circ_0027491	chr12:68816812-68824651	up	46.6090080	4.16513E-05
hsa_circ_0006215	chr3:27437388-27448797	up	45.1249297	3.48496E-05
hsa_circ_0008725	chr21:33426884-33432871	up	37.9178333	0.00010156
hsa_circ_0008156	chr20:3218517-3218994	up	35.2323946	9.53722E-05
hsa_circ_0001460	chr4:177353308-177360677	up	33.9274564	1.77482E-06
hsa_circ_0003600	chr1:204112915-204117707	up	33.3669232	1.99315E-05
novel_circRNA	chr12:1289852-1410453	down	118.537989	1.51102E-10
hsa_circ_0125149	chr4:118105018-118143684	down	116.910157	8.64732E-11
hsa_circ_0008278	chr2:120127688-120175004	down	89.8932136	5.45085E-13
hsa_circ_0092765	chr10:115120185-115215880	down	84.9388758	5.35921E-08
novel_circRNA	chrX:140783176-140784660	down	65.6330435	1.04052E-06
novel_circRNA	chr10:115120185-115241725	down	65.5216704	2.25591E-07
hsa_circ_0131934	chr6:54149056-54230917	down	63.4354473	0.000102382
novel_circRNA	chr10:115120185-115268444	down	54.9719622	1.41497E-06
hsa_circ_0007294	chr12:99772922-99782097	down	54.4268391	4.44801E-08
novel_circRNA	chr7:137463489-137609609	down	52.4703603	0.001182432